Research Article

EGFR inhibition stabilizes cardiomyocyte cohesion in a murine arrhythmogenic cardiomyopathy model

Condensed title: Positive adhesiotropy by EGFR inhibition

Maria Shoykhet[1], Orsela Dervishi[1], Philipp Menauer[1], Matthias Hiermaier[1], Jens Waschke[1] and Sunil Yeruva[1*]

[1]Faculty of Medicine, Ludwig-Maximilian-University (LMU) Munich, Munich, Germany

Corresponding author:

*Sunil Yeruva, Anatomical Institute, Department I – Vegetative Anatomy, Ludwig-Maximilian-University, Pettenkoferstraße 11, 80336 Munich, Germany; Phone: +49-89-2180-72703; sunil.yeruva@med.uni-muenchen.de

Key Words:

Epidermal growth factor receptor, erlotinib, desmoglein 2, desmoplakin, arrhythmogenic cardiomyopathy

Conflict of Interest

The authors declare that no conflict of interest exists.

Abstract

The epidermal growth factor receptor (EGFR) is a ubiquitously expressed receptor tyrosine kinase, which is dysregulated in several kinds of cancer and heart diseases. Arrhythmogenic cardiomyopathy (AC) is a familial heart disease in part caused by impaired desmosome turnover. Thus, stabilization of desmosome integrity, may provide potential new treatment options. Desmosomes, apart from cellular cohesion, provide the structural framework of a signaling hub. Here, we investigated the role of EGFR inhibition on cardiomyocyte cohesion under physiological and pathophysiological conditions using the murine plakoglobin knockout AC model, in which EGFR was upregulated. EGFR inhibition led to enhanced cardiomyocyte cohesion. Immunoprecipitation showed an interaction of EGFR and desmoglein 2 (DSG2). Immunostaining and AFM revealed enhanced DSG2 localization and binding at cell borders upon EGFR inhibition. Enhanced area composita length and desmosome assembly was observed upon EGFR inhibition, confirmed by enhanced DSG2 and desmoplakin (DP) recruitment to the cell borders. Thus, inhibiting EGFR, thereby stabilizing desmosome integrity, may provide new treatment options for AC.

Abbreviation	full form
AC	arrhythmogenic cardiomyopathy
AFM	atomic force microscopy
BSA/NGS	bovine serum albumin and normal goat serum
DES	desmin
DP	desmoplakin
DSC2	desmocollin 2
DSG2	desmoglein 2
EGFR	epidermal growth factor receptor
Erlo	erlotinib
FRAP	fluorescence recovery after photobleach
IgG hc	IgG heavy chain
Jup	junctional plakoglobin
N-CAD	N-Cadherin
NT	non-target
PFA	paraformaldehyde
PG	plakoglobin
PKP2	plakophilin 2
SRC	proto-oncogene kinase Src
STED	stimulated emission depletion
WGA	wheat germ agglutinin
τ	tau; halftime of recovery

39

Introduction

The epidermal growth factor receptor (EGFR) is a ubiquitously expressed transmembrane receptor tyrosine kinase. Dysregulation of EGFR signaling often results in pathologies, such as different kinds of cancer, but also inflammatory skin and bowel disease or other skin, inflammatory or renal disorders (Bhargava et al., 2005, Kleinschmidt-DeMasters et al., 2005, Shia et al., 2005, da Cunha Santos et al., 2011, Campbell et al., 2014, Harskamp et al., 2016, Iwamoto et al., 2019). Today, EGFR inhibitors, either small inhibitory molecules (e.g., erlotinib, gefitinib or lapatinib) or inhibitory antibodies (e.g., cetuximab or panitumumab) are approved as medication to treat non-small cell lung cancer, pancreatic cancer, breast cancer, colorectal carcinoma or squamous cell carcinoma of head and neck (Westover et al., 2018, Sabbah et al., 2020). EGFR can be transactivated through G protein-coupled receptors via second messengers, several protein kinases or matrix metalloproteases (Noma et al., 2007, Makki et al., 2013). In addition, EGFR signaling can be activated, enhanced and mediated by the proto-oncogene tyrosine-protein kinase Src (SRC) (Chen et al., 2018). Vice versa, SRC can be activated by EGFR (Wilde et al., 1999). In the heart, EGFR was found to play a crucial role in cell metabolism, proliferation, cell survival, as well as hypertrophy and remodeling (Stroedecke et al., 2021). EGFR inhibition can lead to heart failure in the healthy heart, and a total knockout of the receptor can lead to severe hypertrophy and hypotension (Schreier et al., 2013, Kenigsberg et al., 2017, Guo et al., 2021). However, under pathological conditions, EGFR inhibition can be cardioprotective, as EGFR has been shown to be upregulated in a diabetic setting (Matrougui, 2010), while EGFR inhibition protected vasculature and heart from diabetes-induced damages (Belmadani et al., 2008, Benter et al., 2009, Akhtar et al., 2012, Choi et al., 2012, El-Hashim et al., 2017). Furthermore, recent studies indicate that EGFR inhibition has a protective effect on cardiomyocytes in hypoxic conditions, i.e., after myocardial infarctions (Heliste et al., 2021). It seems that like in other tissues, EGFR signaling is tightly controlled in the heart, and due to its double role and the multitude of its

downstream effectors, any alterations in EGFR signaling can have severe effects on heart function (Shraim et al., 2021, Forrester et al., 2016).

Arrhythmogenic cardiomyopathy (AC) is a disease most commonly caused by mutations in genes coding for desmosomal proteins, such as desmoglein 2 (DSG2), plakoglobin (PG), desmoplakin (DP), desmocollin 2 (DSC2), N-Cadherin (N-CAD) and plakophilin 2 (PKP2) (Gerull and Brodehl, 2020, Corrado et al., 2017), hence considered as a disease of the desmosome. Causative mutations of AC often lead to alterations in desmosomal contacts between cells, thereby weakening cellular cohesion. Several pathways regulating cardiomyocyte cohesion have been identified so far (Genet et al., 2012, Schlipp et al., 2014, Schinner et al., 2017, Zhao et al., 2019, Shoykhet et al., 2020). Furthermore, there is increasing evidence that desmosomes not only provide cellular cohesion, but also act as signaling hubs (Waschke, 2019, Muller et al., 2021), meaning that desmosomes can influence, but are also influenced by cellular signaling processes. Recent advancement in research suggests that similar molecular mechanisms are present in AC and pemphigus, an autoimmune skin disease, as well as inflammatory bowel diseases (Waschke, 2019, Shoykhet et al., 2020, Schmitt and Waschke, 2021, Yeruva and Waschke, 2022).

EGFR inhibition led to increased cellular cohesion in keratinocytes (Walter et al., 2019), whereas in squamous carcinoma cell lines, EGFR inhibition increased protein levels of DSG2 and DSC2 (Lorch et al., 2004). However, EGFR inhibition by erlotinib in intestinal epithelial cells caused a decrease in cellular cohesion (Ungewiss et al., 2018), revealing that the role of EGFR can vary between different cells or tissues.

EGFR seems to play a major role in the heart function. Furthermore, links between EGFR and DSG2 and other desmosomal proteins have been established. Thus, in this study, we investigated whether inhibition of the EGFR signaling pathway can be used as a therapeutic option for AC, via regulating cardiomyocyte cohesion, using a *Jup*$^{-/-}$ mouse model, which we characterized previously (Schinner et al., 2017, Schinner et al., 2020, Shoykhet et al., 2020).

To this end, we used the well-known and clinically approved first-generation EGFR inhibitor erlotinib and an EGFR signaling molecule SRC inhibitor, PP2. Erlotinib was used to directly inhibit EGFR and PP2 to indirectly inhibit EGFR, by inhibiting the EGFR signaling pathway, since SRC acts both up- and downstream of EGFR. This approach was used as a proof of concept that EGFR inhibition, either using drug or a signaling inhibitor, rescues impaired cardiomyocyte cohesion.

Results

Inhibition of EGFR or SRC lead to positive adhesiotropy in HL-1 cardiomyocytes and murine cardiac slice cultures

In keratinocytes and intestinal epithelial cells, as well as in cancer cells, it is known that EGFR can modulate the desmosomal structure, assembly and signaling and vice versa (Lorch et al., 2004, Klessner et al., 2009, Bektas et al., 2013, Kamekura et al., 2014, Ungewiss et al., 2018). We used the cardiomyocyte-specific plakoglobin knockout ($Jup^{-/-}$) mouse, representing a pathogenic AC model, which shows fibrotic replacement of myocardial tissue as well as arrhythmias (Schinner et al., 2020, Schinner et al., 2017, Shoykhet et al., 2020) and found an upregulation of EGFR protein in the $Jup^{-/-}$ mice as compared to wild type ($Jup^{+/+}$) mice (Figure 1A and Supplementary Figure 1A). Thus, we investigated the role of EGFR in cardiomyocyte cohesion. To this end, we inhibited EGFR directly using erlotinib or SRC, thereby inhibiting the EGFR pathway, using PP2 and performed dispase-based dissociation assays with HL-1 cardiomyocytes and murine cardiac slice cultures. Therefore, treated HL-1 cell monolayers or murine cardiac slices were incubated with a mixture of dispase II and collagenase and mechanical stress was applied to challenge cell-cell contacts, upon which fragments of the monolayer (for HL-1 cells) or single cardiomyocytes (for murine cardiac slices) resulted. The results from this assay shall be interpreted as the lesser the number of fragments or single cardiomyocytes, the higher the cardiomyocyte cohesion or vice versa.

We observed that both EGFR and SRC inhibition enhanced cardiomyocyte cohesion, which we term as positive adhesiotropy, in HL-1 cardiomyocytes and murine cardiac slice cultures (Figure 1B and 1C). Inhibition of EGFR or SRC by erlotinib or PP2, respectively, was confirmed by assessing the phosphorylation levels of their downstream targets: ERK and EGFR (Supplementary Figure 1B-D). We also performed immunostaining of N-CAD and DSG2 in HL-1 cardiomyocytes and found an increase of DSG2 at the cell borders after EGFR or SRC inhibition, compared to controls (Figures 1D and 1E). Next, to assess whether EGFR is in a complex with desmosomal proteins, we immunoprecipitated DSG2 from HL-1 lysates and performed immunoblots for EGFR, PG, DP and PKP2. Indeed, EGFR was found in complex with DSG2 in addition to PG, DP and PKP2 (Figure 1F). Nevertheless, treatment with erlotinib did not alter the composition of this complex.

These experiments showed that inhibition of either EGFR or SRC leads to positive adhesiotropy in HL-1 cardiomyocytes and murine cardiac slice cultures, paralleled by enhanced DSG2 localization along cell junctions.

Inhibition of EGFR increases the DSG2 binding event frequency at cell borders

Since we observed an increase in DSG2 localization at the membrane after EGFR or SRC inhibition, we assessed the role of DSG2 in strengthening cellular cohesion upon EGFR inhibition in cardiomyocytes. For this, we performed atomic force microscopy (AFM) measurements using HL-1 cardiomyocytes. Here, a cantilever with a protein-coated tip approached the cells, where the protein at the tip could eventually interact with proteins at the cell surface. We measured the binding frequency of DSG2, DSC2, or N-CAD-coated tips, as well as the unbinding forces at cell borders and cell surfaces. The areas were chosen using a topography image of the cells, acquired in the force-based quantitative imaging mode (Supplementary Figure 2). We observed an increase in binding frequency at cell borders for DSG2-coated tips only (Figure 2A). In the case of N-CAD coated tips no change in binding frequency was observed (Figure 2B). However, in the case of DSC2-coated tips, reduced

binding frequency at the cell surface, but not the cell border, was found (Figure 2C). On the other hand, no changes in unbinding forces for any of the proteins analyzed were observed (Figure 2D-F). These data indicate that enhanced binding frequency of DSG2 correlates with the strengthening of intercellular adhesion in HL-1 cardiomyocytes upon EGFR inhibition.

Apart from DSG2, positive adhesiotropy induced by EGFR or SRC inhibition is also dependent on DP

To further understand the mechanism of erlotinib or PP2-induced positive adhesiotropy, we performed siRNA-mediated knockdown in HL-1 cardiomyocytes. Firstly, we knocked down *Egfr*, which did not alter cellular cohesion (Figure 3A and Supplementary Figure 3A). We then knocked down *Egfr* and treated the cells with erlotinib or PP2. Upon *Egfr* knockdown, erlotinib-induced positive adhesiotropy was abolished, confirming that the effect observed after erlotinib treatment is mediated through EGFR. Interestingly, SRC inhibition was still effective after *Egfr* knockdown, indicating that the PP2 effect is either independent of EGFR or that SRC is downstream of EGFR (Figure 3B and Supplementary Figure 3A). Next, we knocked down *Dsp* or *Dsg2*. Western blots confirmed all knockdowns (Figure 3C). Knocking down *Dsp* or *Dsg2* did not alter cellular cohesion (Figure 3D and Supplementary Figure 3B and 3C), as observed before (Shoykhet et al., 2020, Schinner et al., 2020). Both, erlotinib and PP2 enhanced cellular cohesion after *Dsg2* knockdown. This suggests that the remaining DSG2 protein might be sufficient enough to mediate the positive adhesiotropic effect of EGFR or SRC inhibition. In previous reports inhibition of EGFR enhanced DP expression in breast cancer cells and led to enhanced DP at the cell border in oral squamous cell carcinoma cells (Lorch et al., 2004, Pang et al., 2004), therefore, we knocked down *Dsp*. EGFR or SRC inhibition-mediated positive adhesiotropy was abrogated upon *Dsp* knockdown, indicating the crucial role of DP in erlotinib or PP2-mediated positive adhesiotropy (Figure 3E and Supplementary Figure 3C). These data highlight the role of DP, along with DSG2, in positive adhesiotropy induced by EGFR or SRC inhibition.

EGFR or SRC inhibition leads to increased area composita length in HL-1 cardiomyocytes

Since both, DSG2 and DP seem to be involved in the positive adhesiotropy induced by EGFR or SRC inhibition, we next performed immunostaining of these proteins together with Phalloidin to stain the cortical actin cytoskeleton. Confocal microscopy images revealed an increase in the localization of DP and DSG2 at cell borders after inhibition of EGFR or SRC (Figure 4A-C). At the same time DSG2 and DP staining looked enlarged in erlotinib and PP2-treated cells compared to vehicle controls, which indicated changes at the area composita, that were shown to be present in intercellular junctions of HL-1 cells (Schlipp et al., 2014). Therefore, we performed stimulated emission depletion (STED) imaging for DSG2 and DP, which showed that area composita number remained unchanged, whereas the area composita length increased after EGFR or SRC inhibition (Figure 4D-F). Apart from that, we observed an increase in desmin (DES) insertion into areae compositae upon treatment with erlotinib or PP2 (Supplementary Figure 4).

Enhanced DP and DSG2 staining in murine cardiac slices after EGFR or SRC inhibition

To confirm the findings from HL-1 cardiomyocytes in a mouse model, we performed immunostaining of murine cardiac slice cultures, both in *Jup*$^{+/+}$ and in *Jup*$^{-/-}$ mice. As observed before (Yeruva et al., 2020), DSG2 was less expressed in the ICDs of *Jup*$^{-/-}$ mice compared to *Jup*$^{+/+}$ mice (Figure 5A and D). No changes in staining intensity or ICD lengths between mediator-treated and untreated slice cultures were found in murine cardiac slice cultures from *Jup*$^{+/+}$ or *Jup*$^{-/-}$ mice. Nonetheless, both DP and DSG2 staining were broader after EGFR or SRC inhibition (Figure 5A-C). Interestingly, in cardiac slices obtained from *Jup*$^{-/-}$ mice, only DSG2 staining width was increased after EGFR or SRC inhibition, whereas changes in DP staining width were not observed (Figure 5D-F). Measurement of staining width is exemplified in Supplementary Figure 5. Taken together, immunostaining showed increased DSG2 and DP localization at cellular junctions after EGFR or SRC inhibition.

EGFR or SRC inhibition promotes desmosomal assembly in HL-1 cardiomyocytes

195 Since the localization of DSG2 at cell borders was increased after EGFR or SRC inhibition,
196 we wondered whether EGFR inhibition alters DSG2 mobility. Therefore, we transfected HL-1
197 cardiomyocytes with a DSG2-GFP construct and performed fluorescence recovery after
198 photobleach (FRAP) experiments. However, we found no changes neither in the halftime of
199 recovery (τ), nor in the immobile fraction after EGFR inhibition (Figures 6A and 6B).
200 Furthermore, we did not observe significant protein localization changes between cytosolic
201 and membrane-bound fractions in Triton-X-100 assays (Supplementary Figure 6A and 6B).
202 Therefore, we next studied desmosomal assembly and performed a Ca^{2+}-switch assay by
203 depleting cells of Ca^{2+} for 90 minutes, using the Ca^{2+}-chelator EGTA to disrupt desmosomes.
204 We performed dispase-based dissociation assays after changing the medium to Ca^{2+}-
205 containing medium together with erlotinib or PP2. EGFR or SRC inhibition led to increased
206 cellular cohesion after a Ca^{2+}-switch, indicating increased desmosomal assembly (Figure 6C
207 and Supplementary Figure 6C). Indeed, immunostaining for DP and DSG2 revealed that both
208 EGFR and SRC inhibition led to enhanced recruitment of DP and DSG2 to the cell borders
209 after the Ca^{2+}-switch in HL-1 cardiomyocytes (Figure 6D-F). Immunoprecipitation of DP
210 after EGFR and SRC inhibition revealed more association of PG and DP in HL-1
211 cardiomyocytes, while PKP2 and DSG2 association with DP was only increased upon SRC
212 inhibition (Figure 6G). These data confirmed that EGFR and SRC inhibition led to enhanced
213 desmosomal assembly.

214 **Discussion**

215 AC is a disease with complex pathogenicity, which at least in part is caused by disturbed
216 desmosome turnover (Liang et al., 2021). The current therapeutic options for AC patients
217 include changes in lifestyle, treatment with antiarrhythmic drugs, catheter ablation,
218 implantable cardiac defibrillator, and end-stage heart transplantation (Corrado et al., 2017).
219 However, in patients carrying mutations in genes coding for proteins of the desmosomal
220 complex, lifestyle changes, such as restraining from physical endurance activities and β-

221 blocker therapy are most commonly used (Corrado et al., 2017). In our previous work, we
222 discovered adrenergic signaling via PKA-mediated PG-phosphorylation at serine 665 as a
223 driving force for DSG2-mediated enhanced cardiomyocyte cohesion, which we termed
224 positive adhesiotropy (Schlipp et al., 2014, Schinner et al., 2017, Shoykhet et al., 2020). This
225 indicated that cardiomyocyte adhesion at ICDs is precisely regulated and can be enhanced via
226 drugs. Because EGFR inhibitors are used in clinics for the treatment of different kinds of
227 cancers (Westover et al., 2018, Sabbah et al., 2020), in this work, we characterized the role of
228 EGFR on cardiomyocyte cohesion and the efficacy of erlotinib to modulate adhesion. Indeed,
229 we show that inhibition of EGFR and its effector molecule, SRC, in HL-1 cardiomyocytes
230 and murine cardiac slice cultures from *Jup*$^{+/+}$ or *Jup*$^{-/-}$ mice enhanced cardiomyocyte
231 cohesion, paralleled by increased desmosome assembly into the area composita (Figure 7).
232 As a first step, we analyzed the expression of EGFR in *Jup*$^{+/+}$ or *Jup*$^{-/-}$ mice hearts and found
233 an increase in EGFR expression in the hearts of *Jup*$^{-/-}$ mice. To our knowledge, this is the first
234 instant of finding EGFR overexpression in murine models of AC. In fact, EGFR activation
235 and signaling was shown to promote TGF-β dependent renal fibrosis (Chen et al., 2012,
236 Samarakoon et al., 2013). Since in AC, replacement of myocardium with fibrotic tissue is a
237 common phenomenon (Corrado et al., 2017), we believe that the observed EGFR
238 overexpression might be related to fibrosis observed in *Jup*$^{-/-}$ mice (Shoykhet et al., 2020,
239 Yeruva et al., 2020, Schinner et al., 2017). It has been shown that upon treatment with the
240 EGFR inhibitor gefitinib, inflammation and hypertrophy caused by chronic treatment with the
241 adrenergic mediator isoprenaline, was ameliorated in mice (Grisanti et al., 2015, Talarico et
242 al., 2014). Moreover, increased EGFR expression was positively correlated with the size of
243 atherosclerotic plaques (Lamb et al., 2004). However, mice with a strong downregulation of
244 EGFR in the heart, have severe hypertrophy and hypotension (Schreier et al., 2013).
245 We used erlotinib or PP2 to inhibit EGFR and SRC kinases, respectively, and focused more
246 on erlotinib, since it is a clinically approved drug. Dispase-based dissociation assays using

247 erlotinib and PP2 in HL-1 cardiomyocytes and murine cardiac slice cultures from *Jup*$^{+/+}$ or
248 *Jup*$^{-/-}$ mice revealed that both the inhibitors enhance cardiomyocyte cohesion. Similar to our
249 findings in this study, EGFR inhibition has been shown to increase cellular cohesion in
250 squamous cell carcinomas (Lorch et al., 2004), whereas in keratinocytes EGFR inhibition
251 protected against DSG3 autoantibody-induced loss of keratinocyte adhesion (Walter et al.,
252 2019). Immunoprecipitation revealed EGFR along with PKP2, DP and PG being in a complex
253 with DSG2. In intestinal epithelial cells, as well as in a cell-free AFM setting, an interaction
254 of DSG2 and EGFR has been observed (Ungewiss et al., 2018). However, to our knowledge
255 in cardiomyocytes this complex was not known before. It has been very well demonstrated
256 that desmosomes in the epithelia or ICDs in the cardiomyocytes not only provide cellular
257 cohesion but can also be part of a signaling hub (Broussard et al., 2015, Najor et al., 2017,
258 Muller et al., 2021, Yeruva and Waschke, 2022), thus disrupting EGFR signaling in this
259 context might lead to changes at the desmosome.
260 On a single molecule level in an AFM setting, we found that binding events mediated by
261 DSG2, but not DSC2 and N-CAD were increased after erlotinib treatment in HL-1
262 cardiomyocytes. Increased binding frequency at the cell borders indicates an increased
263 binding partner localization towards the cell borders. However, it might also be that active
264 EGFR is disturbing the interaction possibility of the binding partner with the DSG2-coated
265 AFM tip, which is restored upon EGFR inhibition. In a cell-free AFM setting DSG2 does not
266 only interact homophilically with DSG2, but also heterophilically with DSC2 (Fuchs et al.,
267 2022). In the AFM setting, only interactions with "free" proteins can be measured. Since we
268 observed an increase of DSG2 at the cell borders upon EGFR inhibition, we suppose that the
269 increased binding frequency at cell borders, in line with our results from the Ca^{2+}-switch
270 assays indicate increased desmosomal assembly, where freshly assembled desmosomal
271 precursors are available for interaction with the opposite cell DSG2 or DSC2. At the same
272 time, the decrease of DSC2 binding frequency might indicate that either DSC2 or its binding

partners are not available for interactions with the DSC2-coated tips, especially at the cell surface. Since we did not observe any significant changes in the DSC2 binding frequency at the cell border, we assumed that the observed decrease in DSC2 binding frequency at cell surface was not off significant concern.

When we knocked down *Egfr* by siRNA, SRC inhibition was still effective in inducing positive adhesiotropy, indicating that the SRC inhibition-mediated effect on cardiomyocyte cohesion is either downstream or at least in part independent of EGFR. However, Western blot analyses revealed that PP2 also caused a significant decrease in EGFR phosphorylation at Y845 and Y1068, indicating SRC acts upstream of EGFR. We have previously shown in keratinocytes that SRC via its target cytoskeletal protein cortactin contributes to the loss of cell cohesion mediated by DSG3 autoantibodies (Kugelmann et al., 2019). Similarly, in cardiomyocytes SRC might also have a direct interaction with desmosomal proteins, independent of the EGFR molecule. Infact, in intestinal epithelial cells DSG2, EGFR and SRC were found to be in one complex (Ungewiss et al., 2018). Upon knockdown of *DSG2*, DSC2 has been shown to be upregulated in colonic adenocarcinoma cell lines (Kamekura et al., 2014), which might explain why we can still observe a positive adhesiotropic effect of EGFR or SRC inhibition upon *Dsg2* knockdown. On the other hand, the remaining DSG2 upon *Dsg2* knockdown could be sufficient to induce positive adhesiotropy after EGFR inhibition. Indeed, we never observed a decrease in cell cohesion upon *Dsg2* knockdown (Schinner et al., 2020, Shoykhet et al., 2020) which further confirms that the partial presence of DSG2 can provide mechanical stability to the cells.

Further, we observed an increased recruitment of DSG2 and DP to the membranes of HL-1 cardiomyocytes, increasing area composita length. The longer areae compositae in HL-1 cardiomyocytes could be the cellular correlate of increased thickness of DSG2 and DP staining in murine cardiac slices. A similar reorganization of ICDs has already been observed in electron microscopy upon adrenergic signaling, which also induces positive adhesiotropy in

cardiomyocytes (Yeruva et al., 2020). We found that the recruitment of DSG2 and DP into the cellular junctions is not caused by increased mobility, rather by an enhanced desmosomal assembly, which is supported by increased DES insertions into DP. Interestingly, in *Jup*$^{-/-}$ mice, we observed changes in DSG2 but not DP localization at the ICD, indicating that the effect of EGFR and SRC inhibition in intact cardiac tissue is at least in part mediated by PG. Indeed, it was shown previously that in *Jup*$^{-/-}$ keratinocytes, steady-state protein levels and recruitment of desmosome components to the membrane were reduced (Yin et al., 2005).

Mechanistically, PG-phosphorylation at tyrosine residues was shown to be involved in EGFR-induced loss of cell adhesion, which decreased association of PG to DP (Gaudry et al., 2001), and triggered translocation of PG and DP from the membrane towards the cytoplasm (Gaudry et al., 2001, Bektas et al., 2013). Furthermore, EGF-induced phosphorylation of PG could be prevented by EGFR inhibition (Lorch et al., 2004). In consensus with the above studies, an increase in co-immunoprecipitation of PG and PKP2 proteins with DP in HL-1 cardiomyocytes after inhibition of EGFR or SRC was observed in this study. These results further strengthen our hypothesis that desmosomal assembly is increased upon EGFR or SRC inhibition.

Based on our results, we anticipate that short-term EGFR inhibition can be beneficial in the setting of AC. Furthermore, unlike other EGFR inhibitors, reports of adverse cardiac effects after erlotinib treatment are very rare (Kenigsberg et al., 2017, Stuhlmiller et al., 2017, Barish et al., 2019, Nagashio et al., 2021). Taken together, we conclude that inhibiting EGFR, thereby enhancing desmosome assembly stabilizes desmosome integrity. However, further studies, investigating the *in vivo* effect of EGFR inhibition utilizing AC mouse models as well as the effects on electromechanical coupling are needed, which are beyond the scope of current study. Nevertheless, we believe that our study is a first step that paves the way for future studies targeting EGFR inhibition by erlotinib as a treatment option for AC.

Materials and Methods

1.1.Cell culture

HL-1 cells, which are immortalized murine atrial myocyte cells, provided by William Claycomb (LSU Health Sciences Center, New Orleans, USA), were cultured in supplemented medium as described before (Shoykhet et al., 2020). Cells were cultured in medium containing norepinephrine, while for experiments, medium without norepinephrine was used.

1.2.Murine cardiac slice culture

Animal handling was performed in accordance with the guidelines from Directive 2010/63/EU of the European Parliament. Previously characterized 12 week old C57BL6/J wildtype and cardiomyocyte specific *Jup*$^{-/-}$ mice were used for experiments (Schinner et al., 2017, Schinner et al., 2020). In brief, mice with loxP sites flanking exon 1 of the junctional plakoglobin gene (*Jup*) on both alleles (Juptm1.1Glr/J mice, the Jackson Laboratory, Bar Harbor, USA) were bred with mice heterozygous for loxP sites in *Jup* with an expression of the recombinase Cre under the control of cardiac-specific alpha myosin heavy chain promoter (Myh6), which were generated by crossing with B6.FVB-Tg(Myh6-cre)2182Mds/J mice (The Jackson Laboratory). Murine cardiac slice cultures were obtained as described before (Shoykhet et al., 2020) with minor adjustments. In brief, after anesthetizing mice with isoflurane, mice were sacrificed by cervical dislocation, the hearts were collected, put into pre-cooled slicing buffer, embedded in low-melt agarose and sliced with a vibratome (LeicaVT1200S vibratome) into 200 µm sections. For treatments, consecutive slices were used to minimize slice-to-slice variability. After respective treatments, slices were processed for lysate preparation, dispase-based dissociation assays and immunostainings. For immunostainings, slices were embedded in NEG-50™ frozen section medium and stored at -80°C until further processing.

1.3.Mediators and reagents

Samples were treated with mediators for 90 minutes. Erlotinib (Santa Cruz, #sc-202154) was used as an EGFR inhibitor at a final concentration of 2.5 µM. PP2 (Merck, #529573) was

351 used to inhibit the EGFR signaling pathway by inhibiting SRC at a final concentration of 10
352 μM. When a Ca^{2+}-switch was performed, cells were treated with 5 mM EGTA (VWR, #0732)
353 for 90 minutes. Then, medium was changed back to Ca^{2+}-containing medium for 90 minutes
354 and mediators were added at the same time.

355 1.4.Lysate preparation

356 For Western blot analyses, lysates were prepared in SDS lysis buffer with protease and
357 phosphatase inhibitors (cOmplete™ Protease Inhibitor Cocktail, Roche, #CO-RO and
358 PhosStop™, Roche, #PHOSS-RO). In the case of HL-1 cardiomyocytes, the medium was
359 removed after treatments and cells were kept on ice, washed with PBS, scraped into SDS lysis
360 buffer and sonicated. When working with murine cardiac slice cultures, slices were treated,
361 washed with TBS and snap-frozen in liquid nitrogen. To prepare the tissue lysates, SDS lysis
362 buffer was added, the samples were transferred into gentleMACS™ M-tubes (Miltenyi
363 Biotec, #130-093-236) and dissociated using the protein_01_01 program of the
364 gentleMACS™ OctoDissociator (Miltenyi Biotec, #130-095-937).

365 For co-immunoprecipitation experiments, cells were cultured in T75 flasks. After treatments,
366 RIPA lysis buffer (10 mM Na_2HPO_4, 150 mM NaCl, 1% Triton X-100, 0.25% SDS, 1%
367 sodium deoxycholate, pH=7.2) containing protease and phosphatase inhibitors was added to
368 the cells and incubated for 30 minutes on ice on a rocking platform. The lysate was then
369 transferred to gentleMACS™ M-tubes, and dissociated using the protein_01_01 program of
370 the gentleMACS™ OctoDissociator.

371 For Triton assays, cells were washed with ice cold PBS and cells were kept on ice on a
372 rocking platform in Triton buffer (0.5% Triton X-100, 50 mM MES, 25 mM EGTA, 5 mM
373 $MgCl_2$, pH=6.8) with protease and phosphatase inhibitors for 20 minutes. After that, the
374 lysate was transferred to Eppendorf tubes and centrifuged at 4°C for 10 minutes at 15000 g in
375 an Eppendorf 5430R centrifuge. The supernatant containing the Triton-soluble proteins was

376 transferred to a new reaction tube, while the pellets were washed with Triton buffer, dissolved
377 in SDS lysis buffer and sonicated.
378 For all assays, protein concentration was measured using the Pierce™ Protein Assay Kit
379 (Thermo Fisher, #23225) according to the manufacturer's protocol.
380 1.5.Western blot analyses
381 Lysates were denatured in Laemmli buffer and boiled for 10 minutes at 95°C, before being
382 loaded on SDS-PAGE gels. The PageRuler™ Plus Prestained Protein Ladder (Thermo Fisher,
383 #26620) was used as a marker. After electrophoresis, proteins were transferred to a
384 nitrocellulose membrane (Thermo Fisher, #LC2006) using the wet-blot method. Membranes
385 were then blocked in 5% milk/TBST, in case of anti-phospho-EGFR antibodies in 5%
386 BSA/TBST, or in case of anti-DP antibodies in ROTI®Block (Carl Roth, #A151.2). For
387 Western blots with lysates from murine tissue samples, as well as Triton blots, the No-Stain™
388 Protein Labeling Reagent (Thermo Fisher, #A44449) was used as loading control according to
389 the manufacturer's protocol. Following primary antibodies were added overnight at 4°C on a
390 rocking platform: anti-DP (Progen, #61003), anti-DSG1/2 (Progen #61002), anti-phospho-
391 EGFR Y845 (Cell Signaling #2231), anti-phospho-EGFR Y1068 (Cell Signaling, #2234),
392 anti-EGFR (sc-373746 (for HL-1 cardiomyocytes) and ab52894 (for murine tissue)), anti-
393 phospho-ERK1/2 ((E-4) Santa Cruz, #sc-7383), anti-ERK (Cell Signaling, #9102), anti-
394 phospho-PG (S665, self-made as described before (Schinner et al., 2020)), anti-PG ((PG5.1)
395 Progen #61005), anti-PKP2 (Progen, #651167) and anti-α-tubulin ((DM1A), abcam,
396 #ab7291). After washing, membranes were incubated with species-matched, HRP-coupled
397 secondary antibodies (Dianova, #111-035-045 or #115-035-068) diluted in TBST or 5%
398 milk/TBST in case of phospho-EGFR antibodies, and developed using an iBright™ FL1500
399 (Thermo Fisher) developer with SuperSignal™ West Pico PLUS Chemiluminescent Substrate
400 (Thermo Fisher, #34577). All primary antibodies were used at 1:1000 dilutions, apart from
401 phospho-EGFR and EGFR antibodies (1:500), phospho-PG (1:20), anti-PKP2 (1:25) and anti-

402 α-tubulin (1:4000). Quantification was performed using the Image Studio Lite v.5.2 or the
403 iBright™ Analysis Software (Invitrogen).

404 1.6.Dissociation Assays

405 Dissociation assays in HL-1 cardiomyocytes were performed as described before (Shoykhet et
406 al., 2020). In brief: after treatment, medium was removed and Liberase-DH (Sigma-Aldrich,
407 #LIBDH-RO) was added, followed by dispase II (Sigma-Aldrich, #D4693). Cells were
408 incubated at 37°C, 5% CO_2, until the cell monolayers detached from the well bottoms. Then,
409 the enzyme mix was carefully replaced by HBSS and mechanical stress was applied by
410 shaking at 1.31 g for 5 minutes on an orbital shaker (Stuart SSM5 orbital shaker). For better
411 visibility, MTT (Sigma-Aldrich, #M5655) was added to the cells and images were taken to
412 count the number of fragments. The amount of fragmentation serves as an indirect
413 measurement of intercellular cohesion, as fewer fragments suggest a stronger cellular
414 cohesion.

415 Dissociation assays in murine cardiac slices were performed similarly to dissociation assays
416 in HL-1 cardiomyocytes. However, in this case, Liberase-DH and dispase II were added
417 simultaneously for 30 minutes. MTT was added and equal mechanical stress was applied to
418 all samples of an experiment using an electrical pipette. Then, the content of each well was
419 filtered using a 70 µm nylon membrane (PluriSelect, #43-10070-60), and transferred to a
420 gridded 96-well plate. Pictures of the well were taken and stitched together using the
421 AutoStich software (Brown, 2018). For quantification, only the number of viable dissociated
422 cardiomyocytes was counted, distinguishable by their rod shape and the MTT staining. To
423 control variations due to different slice size or location in the ventricle, consecutive slices for
424 control and treatments were used, and treatments were normalized to the respective control
425 slice.

426 1.7.Immunostainings

427 Cells were seeded on coverslips, and fixed with paraformaldehyde (PFA) after respective
428 treatments. 7 µm thick sections of murine cardiac slices were cut with a cryostat
429 (HM500OMV, Microm, Walldorf, Germany), sections were transferred to glass slides and
430 adhered by warming up to 38°C. After PFA fixation, the samples were permeabilized with
431 0.1% Triton-X 100 and blocked with bovine serum albumin and normal goat serum
432 (BSA/NGS). Primary antibodies diluted in PBS were added and incubated overnight at 4°C in
433 a wet chamber. Following primary antibodies were used: anti-DES (abcam, #ab32362), anti-
434 DP (Progen, #61003), anti-DSG2 (Progen, #610121) and anti-N-CAD (BD Transduction
435 Laboratories™, #610921). When working with HL-1 cardiomyocytes, PBS was used for
436 washing steps, while for murine tissue samples, 50 mM NH_4Cl in PBS was used. After
437 washing, species-matched, fluorophore-coupled secondary antibodies ((anti-mouse Alexa
438 Fluor® 488 (Dianova #115-545-003), anti-mouse Cy3 (Dianova 115-165-164) or anti-rabbit
439 Cy5 (Dianova, 111-175-144)) were added for 60 minutes. In the case of wheat germ
440 agglutinin (WGA) or Phalloidin staining (Thermo Fisher, #W11261 and Thermo Fisher,
441 #A12379), the dye was added together with the secondary antibodies. WGA was used at 2
442 µg/ml and Phalloidin at 130 nM concentrations. During the last 10 minutes of secondary
443 antibody incubation, DAPI (Sigma Aldrich, #D9542, 0.5 µg/ml) was added. After washing,
444 coverslips were mounted on microscope slides using NPG (Sigma-Aldrich, #P3130). Slides
445 were analyzed using a Leica SP5 confocal microscope (Leica, Mannheim, Germany) with a
446 63X oil objective and the LAS-AF software. Z-scans were performed at 0.25 µm thickness
447 spanning the whole cell volume. Colocalization analyses were performed as described before
448 (Shoykhet et al., 2020), in brief: the membrane region was marked as a region of interest
449 (Supplementary Figure 1E). In this region, the amount of stained pixels in the other channel,
450 where colocalization was to be quantified, was measured and a ratio of colocalization at the
451 membrane was calculated.

452 For stimulated emission depletion (STED) immunostainings, a slightly modified staining
453 protocol was used: instead of washing with PBS, cells were washed with 50 mM NH_4Cl in
454 PBS. Primary antibodies were diluted in BSA/NGS and the following secondary antibodies
455 were used: STAR RED anti-rabbit (abberior, #STRED-1002) and Alexa Fluor® 594 anti-
456 mouse (abcam #ab150120), both 1:200 dilution. Slides were mounted with ProLong™
457 Diamond Antifade (Thermo Scientific, #P36961). Samples were analyzed using a STED
458 expert line microscope from Abberior with a 100X oil objective and the Imspector software.
459 For quantification, areas with a "railroad-like" staining of DP were considered as area
460 composita. To quantify DES insertions into the area composita, the number of spots where
461 DES filaments were inserting into the area composita were counted.

462 1.8.Immunoprecipitation

463 For pulldowns, 1 µg of respective antibodies were added to 1.5 mg of protein lysate
464 overnight, and kept at 4°C on a spinning wheel. To rule out unspecific antibody or bead
465 binding, IgG control samples were prepared, in parallel. Therefore, the same amount of
466 protein lysate was used as for pulldowns, however, instead of primary antibody, 1 µg of
467 normal mouse IgG (Merck, #12-371) was added to the samples. Pulldowns were performed
468 with Protein G Dynabeads™ (Thermo Fisher, #10004D), by adding the lysate-antibody mix
469 for 1 hour at 4°C on a spinning wheel to beads prewashed in RIPA buffer with protease and
470 phosphatase inhibitors. Washing steps were performed using a magnetic rack. Then, beads
471 were washed twice with wash buffer 1 (50 mM Tris-HCl, 150 mM NaCl, 0.1 mM EDTA,
472 0.5% Tween20, pH=7.5), thrice with wash buffer 2 (100 mM Tris-HCl, 200 mM NaCl, 2 M
473 Urea, 0.5% Tween20, pH=7.5), and twice with 1% Triton X-100 in PBS. All wash buffers
474 were supplemented with protease and phosphatase inhibitors. After the last wash step, beads
475 were resuspended in Laemmli buffer, denatured for 10 minutes at 95°C, the lysate was
476 separated from the beads using a magnet and loaded on a SDS-PAGE gel for Western blot
477 analyses. 20 µg of total lysate was used as input control for the Western blots.

478 1.9.Atomic Force Microscopy

479 Atomic Force Microscopy (AFM) measurements were performed as described before
480 (Schinner et al., 2017, Shoykhet et al., 2020) using a Nanowizard® III AFM (JPK
481 instruments, Berlin, Germany) with an optical fluorescence microscope (Axio Observer D1,
482 Carl Zeiss) at 37°C. Cantilevers (MLCT AFM Probes, Bruker, Calle Tecate, CA) were
483 functionalized with recombinant proteins as described elsewhere (Ebner et al., 2007). The
484 following recombinant proteins were used: DSC2-Fc, DSG2-Fc (both self-made by Protein A
485 purification of cell culture supernatants from overexpressing CHO cells, as described in
486 (Waschke et al., 2005)) or recombinant N-CAD-Fc (R&D Systems, #6626-NC-50). The
487 canonical pyramidal-shaped D-tip was used. The thermal noise method (Hutter and
488 Bechhoefer, 1993) was used to determine the spring constants of the tips in order to obtain
489 correct values for unbinding forces. For experiments, HL-1 cardiomyocytes were seeded on
490 24 mm glass coverslips. A bright field image of the cells of interest was acquired with a 63X
491 objective. Afterwards an overview picture of an area of interest was taken in the force-based
492 quantitative imaging (QI) mode with the following settings: pulling speed: 50 µm/s, setpoint:
493 0.2 nN, z-length 2.5 µm. Adhesion measurements were performed on cell borders as well as
494 cell surfaces on an area of 1.5 µm x 5.0 µm using the force mapping mode with the following
495 settings: relative setpoint: 0.2 nN, z-length: 2.5 µm, extension speed: 5.0 µm/s, extend and
496 retract delay: 0.1 s. Information of approach and retraction forces was recorded in force-
497 distance curves (FDCs). The resulting FDCs were analyzed using the JPKSPM Data
498 processing software. Binding events are visible by a step in the FDCs, representing the force
499 needed to rupture the binding between the functionalized tip and the binding partner on the
500 cell. Hence, this force is the unbinding force. Unbinding forces were analyzed using the
501 extreme fit distribution in Origin 2017 software.

502 1.10. siRNA-mediated knockdown

503 For siRNA-mediated knockdown, cells were transfected with a transfection reagent,
504 comprised of OptiMEM (Thermo Scientific, #31985070), RNAiMAX (Thermo Scientific
505 #13778150) and the ON-Target siRNA (Dharmacon, siNT #D-001810-10, si*Egfr* L-040411-
506 00-0005, si*Dsg2* #L-042514-01-005, si*Dsp* #L-040653-01-005) according to manufacturer's
507 protocol. Cells were transfected for 24 hours. 72 hours post transfection, medium was
508 changed again. Experiments were performed 84 hours post-transfection. Each knockdown
509 was confirmed by Western blot.

510 1.11. Fluorescence Recovery After Photobleach

511 For Fluorescence Recovery After Photobleach (FRAP) measurements, HL-1 cardiomyocytes
512 were seeded in ibidi 15 µ-Slide 8 Well Glass Bottom chambers (ibidi, #80827). 24 hours after
513 seeding, cells were transfected with 1 µg DSG2-GFP construct as described before (Schinner
514 et al., 2017), using TurboFect (Thermo, #R0531). Images were captured with a Leica SP5
515 confocal microscope (Leica, Mannheim, Germany) with the LAS-AF software starting 60
516 minutes after treatment with the vehicle or erlotinib. Using the Leica FRAP Wizard, 5
517 pictures were taken before bleaching, then an area of interest was bleached with 20 pulses at
518 100% laser intensity for 0.523 s. After that, 60 pictures were taken every second, 20 pictures
519 were taken every 3 seconds and 10 pictures were taken every 10 seconds. Halftime of
520 recovery, as well as immobile fractions, were calculated using the Leica FRAP Wizard.

521 1.12. Imaging and Statistics

522 Images were processed with Adobe Photoshop CS5, Image Studio Lite v.5.2 and ImageJ
523 software. The cartoon was created using BioRender. Statistical analyses were performed using
524 GraphPad Prism 8. Student's *t*-tests or 1-Way ANOVA with Post-hoc tests were applied after
525 outlier removal and are explained in figure legends. Data are represented as mean ± standard
526 deviation. For dissociation assays as well as for quantification of Western blots in HL-1
527 cardiomyocytes, values were normalized to the average control value of all experiments. For

dissociation assays in murine cardiac slices, the number of dissociated cells was normalized to the respective control slice of the same mouse. Significance was assumed for $p \leq 0.05$.

Acknowledgements

This work was supported by the Ludwig-Maximilian-University Munich through the FöFoLe program and the Deutsche Forschungsgemeinschaft (grant WA2474/11-1 to JW). We thank Martina Hitzenbichler, Daniela Kugelmann, Kathleen Plietz, Kilian Skowranek and the AFM tip coating team for their help and technical assistance.

Author contributions

MS, OD, PM and MH acquired the data. MS and SY analyzed the data and drafted the manuscript. All authors proof-read the manuscript. JW and SY made critical revision of the manuscript for important intellectual content, handled supervision and designed the research.

Statements and declarations

Conflict of Interest

The authors declare that no conflict of interest exists.

Ethical Standards

The manuscript does not contain clinical studies or patient data. Animal handling was in accordance with the guidelines from the Directive 2010/63/EU of the European Parliament and approved by the regional government of Upper Bavaria (Gz. ROB-55.2-2532.Vet_02-19-172).

The Paper Explained

PROBLEM: Current treatment strategies for the congenital heart disease, arrhythmogenic cardiomyopathy, which is in part caused by impaired desmosome assembly and turnover, are limited to symptomatic treatment options. These treatments include changes in lifestyle, anti-arrhythmic drugs or the implantation of an implantable cardiac defibrillator. To improve the quality of life of patients, it is necessary to understand the molecular mechanisms leading to

554 the disassembly of desmosomes and the subsequent decreased cellular cohesion and to find
555 possibilities to overcome them.
556 RESULTS: We found that inhibiting EGFR through erlotinib, or the EGFR signaling pathway
557 through inhibition of SRC by PP2 led to increased cardiomyocyte cohesion (positive
558 adhesiotropy). This was paralleled by increased localization of the desmosomal components
559 DSG2 and DP at the cell borders and enhanced desmosomal assembly.
560 IMPACT: This study paves the way for further studies investigating a novel therapeutic
561 approach for treatment of arrhythmogenic cardiomyopathy by inhibiting EGFR through the
562 clinically approved drug erlotinib.
563
564

565 **Figure 1** EGFR or SRC inhibition induces positive adhesiotropy in cardiomyocytes

566 **A**: Representative Western blot showing protein expression of EGFR and PG in *Jup*$^{+/+}$ and
567 *Jup*$^{-/-}$ mice. **B**: Dispase-based dissociation assay in HL-1 cardiomyocytes upon inhibition of
568 EGFR or SRC by erlotinib or PP2, respectively, with representative pictures of the wells, * p
569 ≤ 0.05 ($p=0.0003$ for erlotinib and $p<0.0001$ for PP2), 1-way ANOVA with Holm-Sidak
570 correction, N=7 biological replicates. **C**: Dispase-based dissociation assay in murine cardiac
571 slice cultures obtained from *Jup*$^{+/+}$ and *Jup*$^{-/-}$ mice upon inhibition of EGFR or SRC, * $p \leq$
572 0.05 (*Jup*$^{+/+}$ mice: $p=0.0012$ for DMSO vs erlotinib and $p=0.0024$ for DMSO vs PP2. *Jup*$^{-/-}$
573 mice: $p=0.0322$ for DMSO vs erlotinib and PP2), 1-way ANOVA with Holm-Sidak
574 correction, N=7 for Jup$^{+/+}$ mice and N=6 for *Jup*$^{-/-}$ mice. **D**: Maximum projections of
575 immunostainings in HL-1 cardiomyocytes for N-CAD and DSG2 showing an increase of
576 DSG2 at the cell borders after erlotinib or PP2 treatments. Z-scans spanning the whole cell
577 volume, z-steps = 0.25 µm. White arrows indicate areas of increased DSG2 localization at the
578 cell membrane. Scale bar: 10 µm. **E:** Quantification of colocalization of N-CAD and DSG2 in
579 HL-1 cardiomyocytes, * $p \leq 0.05$ ($p<0.0001$ for erlotinib and $p=0.0042$ for PP2 compared to
580 DMSO), 1-way ANOVA with Holm-Sidak correction. Each data point represents one
581 individual cell border, N=5 biological replicates. **F:** Representative Western blots for
582 immunoprecipitation of DSG2, co-immunoprecipitation of DP, EGFR, PKP2 and PG, IgG
583 heavy chain (IgG hc) served as loading control for immunoprecipitated samples, N=3
584 biological replicates.

585

586 **Figure 2** EGFR inhibition leads to increased DSG2 binding frequency at cell borders

587 **A-C**: Binding frequency and topography during atomic force microscopy (AFM)
588 measurements on HL-1 cardiomyocytes before and after erlotinib treatment at or close to cell
589 borders and cell surfaces with tips coated with **A**: DSG2, **B**: N-CAD, **C**: DSC2.
590 Measurements were first performed in 90 minutes DMSO-treated samples, then medium was

591 changed, erlotinib was added and experiment was performed after 90 minutes. Green dots in
592 topography images indicate binding events; cyan dots indicate cell borders. Topography
593 images are 1.5 µm x 5 µm. In the graphs, per data-point, 1500 curves were analysed across
594 two areas (1.5 µm x 5 µm). * $p \leq 0.05$. Statistical significance was calculated between DMSO
595 vs erlotinib. (DSG2: cell borders p=0.0426, cell surface: p=0.0785; N-CAD: cell borders
596 p=0.433, cell surface: p=0.1357; DSC2: cell borders p=0.1151, cell surface: p=0.041),
597 unpaired Student's *t*-test, N=3 biological replicates. **D-F**: Unbinding forces measured during
598 AFM measurements on HL-1 cardiomyocytes before and after erlotinib treatment at cell
599 borders and cell surfaces with tips coated with **D**: DSG2, **E**: N-CAD, **f**: DSC2. Per data-point,
600 1500 curves were analysed across two areas (1.5 µm x 5 µm). * $p \leq 0.05$. Statistical
601 significance was calculated between control vs erlotinib. (DSG2 cell borders 0.9808, cell
602 surface p=0.9722; N-CAD: p=0.5380, cell surface p=0.958; DSC2: p=0.9258, cell surface
603 p=0.4421), unpaired, Student's *t*-test, N=3 biological replicates.
604
605 **Figure 3** Positive adhesiotropy induced by EGFR or SRC inhibition is dependent on DP
606 **A**: Dispase-based dissociation assay in HL-1 cardiomyocytes after siRNA-mediated
607 knockdown of EGFR and non-target (NT) control knockdown. Unpaired Student's *t*-test
608 (p=0.9858), N=6 biological replicates. **B**: Dispase-based dissociation assay in HL-1
609 cardiomyocytes after siRNA-mediated knockdown of EGFR and treatments with erlotinib or
610 PP2. *$p \leq 0.05$ (siNT: p=0.0264 for DMSO vs erlotinib and PP2; siEGFR: p=0.8257 for
611 DMSO vs erlotinib and p=0.0494 for DMSO vs PP2), 1-way ANOVA with Holm-Sidak
612 correction, N=6. **C**: Representative Western blot confirmation of siRNA-mediated
613 knockdown efficiency for EGFR, DP and DSG2, α-tubulin served as a loading control, N=6
614 biological replicates. **D**: Dispase-based dissociation assay in HL-1 cardiomyocytes after
615 siRNA-mediated knockdown of DSG2 or DP *$p \leq 0.05$ (p=0.982 for siNT vs siDSG2 and
616 p=0.2204 for siNT vs siDSP), unpaired Student's *t*-test. **E**: Dispase-based dissociation assay

617 in HL-1 cardiomyocytes after siRNA-mediated knockdown of DSG2 or DP and treatments
618 with erlotinib or PP2. *p ≤ 0.05 (siNT: p=0.0002 for DMSO vs erlotinib and p= 0.001 for
619 DMSO vs PP2; siDSG2: p=0.0081 for erlotinib and p=0.0097 for PP2; siDSP: p=0.9512 for
620 erlotinib and PP2), 1-way ANOVA with Holm-Sidak correction, N=6-8 biological replicates.
621
622 **Figure 4** Increased DP and DSG2 recruitment to the cell membranes leads to longer areae
623 compositae upon EGFR or SRC inhibition
624 **A**: Immunostaining of DP and DSG2 in HL-1 cardiomyocytes with Phalloidin as membrane
625 marker. Scale bar: 10 µm. White arrows represent an increase in DSG2 and DP localization to
626 the membrane compared to DMSO. **B**: Quantification of colocalization of DP and Phalloidin.
627 *p ≤ 0.05 (p=0.0001 for DMSO vs erlotinib and p<0.0001 for DMSO vs PP2), 1-way
628 ANOVA with Holm-Sidak correction. **C**: Quantification of colocalization of DSG2 and
629 Phalloidin. *p ≤ 0.05 (p=0.0002 for DMSO vs erlotinib and p=0.0122 for DMSO vs PP2), 1-
630 way ANOVA with Holm-Sidak correction. Each data point represents one individual cell
631 border, N=6 biological replicates. **D**: STED images of HL-1 cardiomyocytes stained for DP
632 and DSG2. Scale bar in overviews: 2 µm, scale bar in zooms: 500 nm. **E**: Number of areae
633 compositae over six areas (15 µm x 15 µm) from N=5 biological replicates, *p ≤ 0.05
634 (p=0.2959 for DMSO vs erlotinib and p=0.6994 for DMSO vs PP2), 1-way ANOVA with
635 Holm-Sidak correction. **F**: Quantification of area composita length. *p ≤ 0.05 (p=0.0078 for
636 DMSO vs erlotinib and p=0.0001 for DMSO vs PP2), 1-way ANOVA with Holm-Sidak
637 correction, N=4 biological replicates.
638
639 **Figure 5** EGFR or SRC inhibition leads to increased recruitment of DP and DSG2 into the
640 ICDs in *Jup*$^{+/+}$ and *Jup*$^{-/-}$ mice
641 **A**: Immunostaining of DP and DSG2 in *Jup*$^{+/+}$ murine cardiac slices with WGA as membrane
642 marker. Scale bar: 8 µm. **B**: DP staining width. **C**: DSG2 staining width. * p ≤ 0.05, (DP

643 staining width: p<0.0001 for DMSO vs erlotinib and PP2; DSG2 staining width: p<0.0001 for
644 DMSO vs erlotinib and p=0.0004 for DMSO vs PP2), 1-way ANOVA with Holm-Sidak
645 correction. Each data point represents one ICD, N=4 mice. **D**: Immunostainings of *Jup*$^{-/-}$
646 murine cardiac slices for DP and DSG2 with WGA as membrane marker. Scale bar: 8 µm. **E**:
647 DP staining width. **F**: DSG2 staining width. * p ≤ 0.05 (DP staining width: p=0.7121 for
648 DMSO vs erlotinib and p=0.5042 for DMSO vs PP2; DSG2 staining width: p=0.0189 for
649 DMSO vs erlotinib and p=0.0147 for DMSO vs PP2), 1-way ANOVA with Holm-Sidak
650 correction. Each data point represents one ICD, N=4 mice. White arrows represent an increase
651 staining width in DSG2 or DP staining compared to DMSO.
652
653 **Figure 6** Increased recruitment of DP and DSG2 towards the cell membrane is achieved by
654 enhanced desmosome assembly
655 **A-B**: Fluorescence recovery after photobleach (FRAP) measurements in HL-1
656 cardiomyocytes transfected with DSG2-GFP and treated with DMSO or erlotinib.
657 Measurements were performed 60-120 minutes post treatment **A**: Immobile fraction **B**:
658 Halftime of recovery (τ). * p ≤ 0.05 (immobile fraction p=0.6933; τ p=0.5252 for DMSO vs
659 erlotinib), unpaired Student's *t*-test, N=4 biological replicates. **C:** Dispase-based dissociation
660 assay in HL-1 cardiomyocytes after 90 minutes of Ca^{2+}-depletion and subsequent Ca^{2+}-
661 repletion together with erlotinib or PP2. *p ≤ 0.05 (p=0.0201 for DMSO vs erlotinib and
662 PP2), 1-way ANOVA with Holm-Sidak correction, N=6 biological replicates. **D:**
663 Immunostaining of DP and DSG2 in HL-1 cardiomyocytes with Phalloidin as membrane
664 marker after 90 minutes of Ca^{2+}-depletion and subsequent Ca^{2+}-repletion together with
665 erlotinib or PP2. White arrows indicate areas of increased DP or DSG2 recruitment to the cell
666 membrane. Scale bar: 10 µm. **E-F:** Quantification of colocalization of **E**: DP or **F**: DSG2 and
667 Phalloidin, * p ≤ 0.05 (DP: p=0.0216 for DMSO vs erlotinib and p=0.0036 for DMSO vs
668 PP2); DSG2: p=0.0073 for erlotinib and p=0.0004 for PP2), 1-way ANOVA with Holm-Sidak

669 correction, N=4 biological replicates. Each data point represents one individual cell border.
670 **G:** Immunoprecipitation of DP from HL-1 lysates, co-immunoprecipitation of EGFR, DSG2,
671 PKP2 and PG, N=3 biological replicates.
672
673 **Fig. 7** Schematic overview of EGFR or SRC inhibition-mediated positive adhesiotropy
674 EGFR exists in complex with DSG2, along with DP, PG and PKP2, either at the cell borders
675 or in the cytoplasm. EGFR or SRC inhibition, via erlotinib or PP2, respectively, led to
676 positive adhesiotropy in cardiomyocytes by enhancing the desmosome assembly, which
677 increased area composita length.
678

679 **References**

680 AKHTAR, S., YOUSIF, M. H., DHAUNSI, G. S., CHANDRASEKHAR, B., AL-FARSI, O. & BENTER, I. F. 2012.
681 Angiotensin-(1-7) inhibits epidermal growth factor receptor transactivation via a Mas
682 receptor-dependent pathway. *Br J Pharmacol,* 165**,** 1390-400.
683 BARISH, R., GATES, E. & BARAC, A. 2019. Trastuzumab-Induced Cardiomyopathy. *Cardiol Clin,* 37**,**
684 407-418.
685 BEKTAS, M., JOLLY, P. S., BERKOWITZ, P., AMAGAI, M. & RUBENSTEIN, D. S. 2013. A pathophysiologic
686 role for epidermal growth factor receptor in pemphigus acantholysis. *J Biol Chem,* 288**,** 9447-
687 56.
688 BELMADANI, S., PALEN, D. I., GONZALEZ-VILLALOBOS, R. A., BOULARES, H. A. & MATROUGUI, K. 2008.
689 Elevated epidermal growth factor receptor phosphorylation induces resistance artery
690 dysfunction in diabetic db/db mice. *Diabetes,* 57**,** 1629-37.
691 BENTER, I. F., BENBOUBETRA, M., HOLLINS, A. J., YOUSIF, M. H., CANATAN, H. & AKHTAR, S. 2009.
692 Early inhibition of EGFR signaling prevents diabetes-induced up-regulation of multiple gene
693 pathways in the mesenteric vasculature. *Vascul Pharmacol,* 51**,** 236-45.
694 BHARGAVA, R., GERALD, W. L., LI, A. R., PAN, Q., LAL, P., LADANYI, M. & CHEN, B. 2005. EGFR gene
695 amplification in breast cancer: correlation with epidermal growth factor receptor mRNA and
696 protein expression and HER-2 status and absence of EGFR-activating mutations. *Mod Pathol,*
697 18**,** 1027-33.
698 BROUSSARD, J. A., GETSIOS, S. & GREEN, K. J. 2015. Desmosome regulation and signaling in disease.
699 *Cell Tissue Res,* 360**,** 501-12.
700 BROWN, M. 2018. *Autostitch Software* [Online]. Available:
701 http://matthewalunbrown.com/autostitch/autostitch.html [Accessed].
702 CAMPBELL, P., MORTON, P. E., TAKEICHI, T., SALAM, A., ROBERTS, N., PROUDFOOT, L. E., MELLERIO,
703 J. E., AMINU, K., WELLINGTON, C., PATIL, S. N., AKIYAMA, M., LIU, L., MCMILLAN, J. R.,
704 ARISTODEMOU, S., ISHIDA-YAMAMOTO, A., ABDUL-WAHAB, A., PETROF, G., FONG, K.,
705 HARNCHOOWONG, S., STONE, K. L., HARPER, J. I., IRWIN MCLEAN, W. H., SIMPSON, M. A.,
706 PARSONS, M. & MCGRATH, J. A. 2014. Epithelial inflammation resulting from an inherited
707 loss-of-function mutation in EGFR. *J Invest Dermatol,* 134**,** 2570-2578.
708 CHEN, J., CHEN, J. K., NAGAI, K., PLIETH, D., TAN, M., LEE, T. C., THREADGILL, D. W., NEILSON, E. G. &
709 HARRIS, R. C. 2012. EGFR signaling promotes TGFbeta-dependent renal fibrosis. *J Am Soc*
710 *Nephrol,* 23**,** 215-24.
711 CHEN, Z., OH, D., DUBEY, A. K., YAO, M., YANG, B., GROVES, J. T. & SHEETZ, M. 2018. EGFR family and
712 Src family kinase interactions: mechanics matters? *Curr Opin Cell Biol,* 51**,** 97-102.
713 CHOI, S. K., GALAN, M., PARTYKA, M., TREBAK, M., BELMADANI, S. & MATROUGUI, K. 2012. Chronic
714 inhibition of epidermal growth factor receptor tyrosine kinase and extracellular signal-
715 regulated kinases 1 and 2 (ERK1/2) augments vascular response to limb ischemia in type 2
716 diabetic mice. *Am J Pathol,* 180**,** 410-8.
717 CORRADO, D., BASSO, C. & JUDGE, D. P. 2017. Arrhythmogenic Cardiomyopathy. *Circ Res,* 121**,** 784-
718 802.
719 DA CUNHA SANTOS, G., SHEPHERD, F. A. & TSAO, M. S. 2011. EGFR mutations and lung cancer. *Annu*
720 *Rev Pathol,* 6**,** 49-69.
721 EBNER, A., WILDLING, L., KAMRUZZAHAN, A. S., RANKL, C., WRUSS, J., HAHN, C. D., HOLZL, M., ZHU,
722 R., KIENBERGER, F., BLAAS, D., HINTERDORFER, P. & GRUBER, H. J. 2007. A new, simple
723 method for linking of antibodies to atomic force microscopy tips. *Bioconjug Chem,* 18**,** 1176-
724 84.
725 EL-HASHIM, A. Z., KHAJAH, M. A., RENNO, W. M., BABYSON, R. S., UDDIN, M., BENTER, I. F.,
726 EZEAMUZIE, C. & AKHTAR, S. 2017. Src-dependent EGFR transactivation regulates lung
727 inflammation via downstream signaling involving ERK1/2, PI3Kdelta/Akt and NFkappaB
728 induction in a murine asthma model. *Sci Rep,* 7**,** 9919.

729 FORRESTER, S. J., KAWAI, T., O'BRIEN, S., THOMAS, W., HARRIS, R. C. & EGUCHI, S. 2016. Epidermal
730 Growth Factor Receptor Transactivation: Mechanisms, Pathophysiology, and Potential
731 Therapies in the Cardiovascular System. *Annu Rev Pharmacol Toxicol,* 56**,** 627-53.
732 FUCHS, M., KUGELMANN, D., SCHLEGEL, N., VIELMUTH, F. & WASCHKE, J. 2022. Desmoglein 2 can
733 undergo Ca(2+)-dependent interactions with both desmosomal and classical cadherins
734 including E-cadherin and N-cadherin. *Biophys J,* 121**,** 1322-1335.
735 GAUDRY, C. A., PALKA, H. L., DUSEK, R. L., HUEN, A. C., KHANDEKAR, M. J., HUDSON, L. G. & GREEN,
736 K. J. 2001. Tyrosine-phosphorylated plakoglobin is associated with desmogleins but not
737 desmoplakin after epidermal growth factor receptor activation. *J Biol Chem,* 276**,** 24871-80.
738 GENET, G., GUILBEAU-FRUGIER, C., HONTON, B., DAGUE, E., SCHNEIDER, M. D., COATRIEUX, C.,
739 CALISE, D., CARDIN, C., NIETO, C., PAYRE, B., DUBROCA, C., MARCK, P., HEYMES, C., DUBRAC,
740 A., ARVANITIS, D., DESPAS, F., ALTIE, M. F., SEGUELAS, M. H., DELISLE, M. B., DAVY, A.,
741 SENARD, J. M., PATHAK, A. & GALES, C. 2012. Ephrin-B1 is a novel specific component of the
742 lateral membrane of the cardiomyocyte and is essential for the stability of cardiac tissue
743 architecture cohesion. *Circ Res,* 110**,** 688-700.
744 GERULL, B. & BRODEHL, A. 2020. Genetic Animal Models for Arrhythmogenic Cardiomyopathy. *Front*
745 *Physiol,* 11**,** 624.
746 GRISANTI, L. A., REPAS, A. A., TALARICO, J. A., GOLD, J. I., CARTER, R. L., KOCH, W. J. & TILLEY, D. G.
747 2015. Temporal and gefitinib-sensitive regulation of cardiac cytokine expression via chronic
748 beta-adrenergic receptor stimulation. *Am J Physiol Heart Circ Physiol,* 308**,** H316-30.
749 GUO, S., OKYERE, A. D., MCEACHERN, E., STRONG, J. L., CARTER, R. L., PATWA, V. C., THOMAS, T. P.,
750 LANDY, M., SONG, J., LUCCHESE, A. M., MARTIN, T. G., GAO, E., RAJAN, S., KIRK, J. A., KOCH,
751 W. J., CHEUNG, J. Y. & TILLEY, D. G. 2021. Epidermal growth factor receptor-dependent
752 maintenance of cardiac contractility. *Cardiovasc Res*.
753 HARSKAMP, L. R., GANSEVOORT, R. T., VAN GOOR, H. & MEIJER, E. 2016. The epidermal growth
754 factor receptor pathway in chronic kidney diseases. *Nat Rev Nephrol,* 12**,** 496-506.
755 HELISTE, J., JOKILAMMI, A., VAPARANTA, K., PAATERO, I. & ELENIUS, K. 2021. Combined genetic and
756 chemical screens indicate protective potential for EGFR inhibition to cardiomyocytes under
757 hypoxia. *Sci Rep,* 11**,** 16661.
758 HUTTER, J. L. & BECHHOEFER, J. 1993. Calibration of atomic-force microscope tips. *Review of*
759 *Scientific Instruments,* 64**,** 1868-1873.
760 IWAMOTO, M., SASO, W., SUGIYAMA, R., ISHII, K., OHKI, M., NAGAMORI, S., SUZUKI, R., AIZAKI, H.,
761 RYO, A., YUN, J. H., PARK, S. Y., OHTANI, N., MURAMATSU, M., IWAMI, S., TANAKA, Y.,
762 SUREAU, C., WAKITA, T. & WATASHI, K. 2019. Epidermal growth factor receptor is a host-
763 entry cofactor triggering hepatitis B virus internalization. *Proc Natl Acad Sci U S A,* 116**,** 8487-
764 8492.
765 KAMEKURA, R., KOLEGRAFF, K. N., NAVA, P., HILGARTH, R. S., FENG, M., PARKOS, C. A. & NUSRAT, A.
766 2014. Loss of the desmosomal cadherin desmoglein-2 suppresses colon cancer cell
767 proliferation through EGFR signaling. *Oncogene,* 33**,** 4531-6.
768 KENIGSBERG, B., JAIN, V. & BARAC, A. 2017. Cardio-oncology Related to Heart Failure: Epidermal
769 Growth Factor Receptor Target-Based Therapy. *Heart Fail Clin,* 13**,** 297-309.
770 KLEINSCHMIDT-DEMASTERS, B. K., LILLEHEI, K. O. & VARELLA-GARCIA, M. 2005. Glioblastomas in the
771 older old. *Arch Pathol Lab Med,* 129**,** 624-31.
772 KLESSNER, J. L., DESAI, B. V., AMARGO, E. V., GETSIOS, S. & GREEN, K. J. 2009. EGFR and ADAMs
773 cooperate to regulate shedding and endocytic trafficking of the desmosomal cadherin
774 desmoglein 2. *Mol Biol Cell,* 20**,** 328-37.
775 KUGELMANN, D., ROTZER, V., WALTER, E., EGU, D. T., FUCHS, M. T., VIELMUTH, F., VARGAS-ROBLES,
776 H., SCHNOOR, M., HERTL, M., EMING, R., ROTTNER, K., SCHMIDT, A., SPINDLER, V. &
777 WASCHKE, J. 2019. Role of Src and Cortactin in Pemphigus Skin Blistering. *Front Immunol,* 10**,**
778 626.
779 LAMB, D. J., MODJTAHEDI, H., PLANT, N. J. & FERNS, G. A. 2004. EGF mediates monocyte chemotaxis
780 and macrophage proliferation and EGF receptor is expressed in atherosclerotic plaques.
781 *Atherosclerosis,* 176**,** 21-6.

782 LIANG, Y., LYON, R. C., PELLMAN, J., BRADFORD, W. H., LANGE, S., BOGOMOLOVAS, J., DALTON, N. D.,
783 GU, Y., BOBAR, M., LEE, M. H., IWAKUMA, T., NIGAM, V., ASIMAKI, A., SCHEINMAN, M.,
784 PETERSON, K. L. & SHEIKH, F. 2021. Desmosomal COP9 regulates proteome degradation in
785 arrhythmogenic right ventricular dysplasia/cardiomyopathy. *J Clin Invest,* 131.
786 LORCH, J. H., KLESSNER, J., PARK, J. K., GETSIOS, S., WU, Y. L., STACK, M. S. & GREEN, K. J. 2004.
787 Epidermal growth factor receptor inhibition promotes desmosome assembly and strengthens
788 intercellular adhesion in squamous cell carcinoma cells. *J Biol Chem,* 279**,** 37191-200.
789 MAKKI, N., THIEL, K. W. & MILLER, F. J., JR. 2013. The epidermal growth factor receptor and its
790 ligands in cardiovascular disease. *Int J Mol Sci,* 14**,** 20597-613.
791 MATROUGUI, K. 2010. Diabetes and microvascular pathophysiology: role of epidermal growth factor
792 receptor tyrosine kinase. *Diabetes Metab Res Rev,* 26**,** 13-6.
793 MULLER, L., HATZFELD, M. & KEIL, R. 2021. Desmosomes as Signaling Hubs in the Regulation of Cell
794 Behavior. *Front Cell Dev Biol,* 9**,** 745670.
795 NAGASHIO, K., TAJIRI, K., SATO, K. & IEDA, M. 2021. Erlotinib-Induced Cardiomyopathy in a Patient
796 with Metastatic Non-Small Cell Lung Cancer. *Int Heart J,* 62**,** 1171-1175.
797 NAJOR, N. A., FITZ, G. N., KOETSIER, J. L., GODSEL, L. M., ALBRECHT, L. V., HARMON, R. & GREEN, K. J.
798 2017. Epidermal Growth Factor Receptor neddylation is regulated by a desmosomal-COP9
799 (Constitutive Photomorphogenesis 9) signalosome complex. *Elife,* 6.
800 NOMA, T., LEMAIRE, A., NAGA PRASAD, S. V., BARKI-HARRINGTON, L., TILLEY, D. G., CHEN, J., LE
801 CORVOISIER, P., VIOLIN, J. D., WEI, H., LEFKOWITZ, R. J. & ROCKMAN, H. A. 2007. Beta-
802 arrestin-mediated beta1-adrenergic receptor transactivation of the EGFR confers
803 cardioprotection. *J Clin Invest,* 117**,** 2445-58.
804 PANG, H., ROWAN, B. G., AL-DHAHERI, M. & FABER, L. E. 2004. Epidermal growth factor suppresses
805 induction by progestin of the adhesion protein desmoplakin in T47D breast cancer cells.
806 *Breast Cancer Res,* 6**,** R239-45.
807 SABBAH, D. A., HAJJO, R. & SWEIDAN, K. 2020. Review on Epidermal Growth Factor Receptor (EGFR)
808 Structure, Signaling Pathways, Interactions, and Recent Updates of EGFR Inhibitors. *Curr Top*
809 *Med Chem,* 20**,** 815-834.
810 SAMARAKOON, R., DOBBERFUHL, A. D., COOLEY, C., OVERSTREET, J. M., PATEL, S., GOLDSCHMEDING,
811 R., MELDRUM, K. K. & HIGGINS, P. J. 2013. Induction of renal fibrotic genes by TGF-beta1
812 requires EGFR activation, p53 and reactive oxygen species. *Cell Signal,* 25**,** 2198-209.
813 SCHINNER, C., OLIVARES-FLOREZ, S., SCHLIPP, A., TRENZ, S., FEINENDEGEN, M., FLASWINKEL, H.,
814 KEMPF, E., EGU, D. T., YERUVA, S. & WASCHKE, J. 2020. The inotropic agent digitoxin
815 strengthens desmosomal adhesion in cardiac myocytes in an ERK1/2-dependent manner.
816 *Basic Res Cardiol,* 115**,** 46.
817 SCHINNER, C., VIELMUTH, F., ROTZER, V., HIERMAIER, M., RADEVA, M. Y., CO, T. K., HARTLIEB, E.,
818 SCHMIDT, A., IMHOF, A., MESSOUDI, A., HORN, A., SCHLIPP, A., SPINDLER, V. & WASCHKE, J.
819 2017. Adrenergic Signaling Strengthens Cardiac Myocyte Cohesion. *Circ Res,* 120**,** 1305-1317.
820 SCHLIPP, A., SCHINNER, C., SPINDLER, V., VIELMUTH, F., GEHMLICH, K., SYRRIS, P., MCKENNA, W. J.,
821 DENDORFER, A., HARTLIEB, E. & WASCHKE, J. 2014. Desmoglein-2 interaction is crucial for
822 cardiomyocyte cohesion and function. *Cardiovasc Res,* 104**,** 245-57.
823 SCHMITT, T. & WASCHKE, J. 2021. Autoantibody-Specific Signalling in Pemphigus. *Front Med*
824 *(Lausanne),* 8**,** 701809.
825 SCHREIER, B., RABE, S., SCHNEIDER, B., BRETSCHNEIDER, M., RUPP, S., RUHS, S., NEUMANN, J.,
826 RUECKSCHLOSS, U., SIBILIA, M., GOTTHARDT, M., GROSSMANN, C. & GEKLE, M. 2013. Loss of
827 epidermal growth factor receptor in vascular smooth muscle cells and cardiomyocytes causes
828 arterial hypotension and cardiac hypertrophy. *Hypertension,* 61**,** 333-40.
829 SHIA, J., KLIMSTRA, D. S., LI, A. R., QIN, J., SALTZ, L., TERUYA-FELDSTEIN, J., AKRAM, M., CHUNG, K. Y.,
830 YAO, D., PATY, P. B., GERALD, W. & CHEN, B. 2005. Epidermal growth factor receptor
831 expression and gene amplification in colorectal carcinoma: an immunohistochemical and
832 chromogenic in situ hybridization study. *Mod Pathol,* 18**,** 1350-6.

833 SHOYKHET, M., TRENZ, S., KEMPF, E., WILLIAMS, T., GERULL, B., SCHINNER, C., YERUVA, S. &
834 WASCHKE, J. 2020. Cardiomyocyte adhesion and hyperadhesion differentially require ERK1/2
835 and plakoglobin. *JCI Insight,* 5.
836 SHRAIM, B. A., MOURSI, M. O., BENTER, I. F., HABIB, A. M. & AKHTAR, S. 2021. The Role of Epidermal
837 Growth Factor Receptor Family of Receptor Tyrosine Kinases in Mediating Diabetes-Induced
838 Cardiovascular Complications. *Front Pharmacol,* 12**,** 701390.
839 STROEDECKE, K., MEINEL, S., MARKWARDT, F., KLOECKNER, U., STRAETZ, N., QUARCH, K., SCHREIER,
840 B., KOPF, M., GEKLE, M. & GROSSMANN, C. 2021. The mineralocorticoid receptor leads to
841 increased expression of EGFR and T-type calcium channels that support HL-1 cell
842 hypertrophy. *Sci Rep,* 11**,** 13229.
843 STUHLMILLER, T. J., ZAWISTOWSKI, J. S., CHEN, X., SCIAKY, N., ANGUS, S. P., HICKS, S. T., PARRY, T. L.,
844 HUANG, W., BEAK, J. Y., WILLIS, M. S., JOHNSON, G. L. & JENSEN, B. C. 2017. Kinome and
845 Transcriptome Profiling Reveal Broad and Distinct Activities of Erlotinib, Sunitinib, and
846 Sorafenib in the Mouse Heart and Suggest Cardiotoxicity From Combined Signal Transducer
847 and Activator of Transcription and Epidermal Growth Factor Receptor Inhibition. *J Am Heart*
848 *Assoc,* 6.
849 TALARICO, J. A., CARTER, R. L., GRISANTI, L. A., YU, J. E., REPAS, A. A. & TILLEY, D. G. 2014. beta-
850 adrenergic receptor-dependent alterations in murine cardiac transcript expression are
851 differentially regulated by gefitinib in vivo. *PLoS One,* 9**,** e99195.
852 UNGEWISS, H., ROTZER, V., MEIR, M., FEY, C., DIEFENBACHER, M., SCHLEGEL, N. & WASCHKE, J. 2018.
853 Dsg2 via Src-mediated transactivation shapes EGFR signaling towards cell adhesion. *Cell Mol*
854 *Life Sci,* 75**,** 4251-4268.
855 WALTER, E., VIELMUTH, F., WANUSKE, M. T., SEIFERT, M., POLLMANN, R., EMING, R. & WASCHKE, J.
856 2019. Role of Dsg1- and Dsg3-Mediated Signaling in Pemphigus Autoantibody-Induced Loss
857 of Keratinocyte Cohesion. *Front Immunol,* 10**,** 1128.
858 WASCHKE, J. 2019. Desmogleins as signaling hubs regulating cell cohesion and tissue/organ function
859 in skin and heart - EFEM lecture 2018. *Ann Anat,* 226**,** 96-100.
860 WASCHKE, J., BRUGGEMAN, P., BAUMGARTNER, W., ZILLIKENS, D. & DRENCKHAHN, D. 2005.
861 Pemphigus foliaceus IgG causes dissociation of desmoglein 1-containing junctions without
862 blocking desmoglein 1 transinteraction. *J Clin Invest,* 115**,** 3157-65.
863 WESTOVER, D., ZUGAZAGOITIA, J., CHO, B. C., LOVLY, C. M. & PAZ-ARES, L. 2018. Mechanisms of
864 acquired resistance to first- and second-generation EGFR tyrosine kinase inhibitors. *Ann*
865 *Oncol,* 29**,** i10-i19.
866 WILDE, A., BEATTIE, E. C., LEM, L., RIETHOF, D. A., LIU, S. H., MOBLEY, W. C., SORIANO, P. & BRODSKY,
867 F. M. 1999. EGF receptor signaling stimulates SRC kinase phosphorylation of clathrin,
868 influencing clathrin redistribution and EGF uptake. *Cell,* 96**,** 677-87.
869 YERUVA, S., KEMPF, E., EGU, D. T., FLASWINKEL, H., KUGELMANN, D. & WASCHKE, J. 2020. Adrenergic
870 Signaling-Induced Ultrastructural Strengthening of Intercalated Discs via Plakoglobin Is
871 Crucial for Positive Adhesiotropy in Murine Cardiomyocytes. *Front Physiol,* 11**,** 430.
872 YERUVA, S. P. & WASCHKE, J. 2022. Structure and regulation of desmosomes in intercalated discs:
873 Lessons from epithelia. *J Anat*.
874 YIN, T., GETSIOS, S., CALDELARI, R., GODSEL, L. M., KOWALCZYK, A. P., MULLER, E. J. & GREEN, K. J.
875 2005. Mechanisms of plakoglobin-dependent adhesion: desmosome-specific functions in
876 assembly and regulation by epidermal growth factor receptor. *J Biol Chem,* 280**,** 40355-63.
877 ZHAO, G., QIU, Y., ZHANG, H. M. & YANG, D. 2019. Intercalated discs: cellular adhesion and signaling
878 in heart health and diseases. *Heart Fail Rev,* 24**,** 115-132.

879

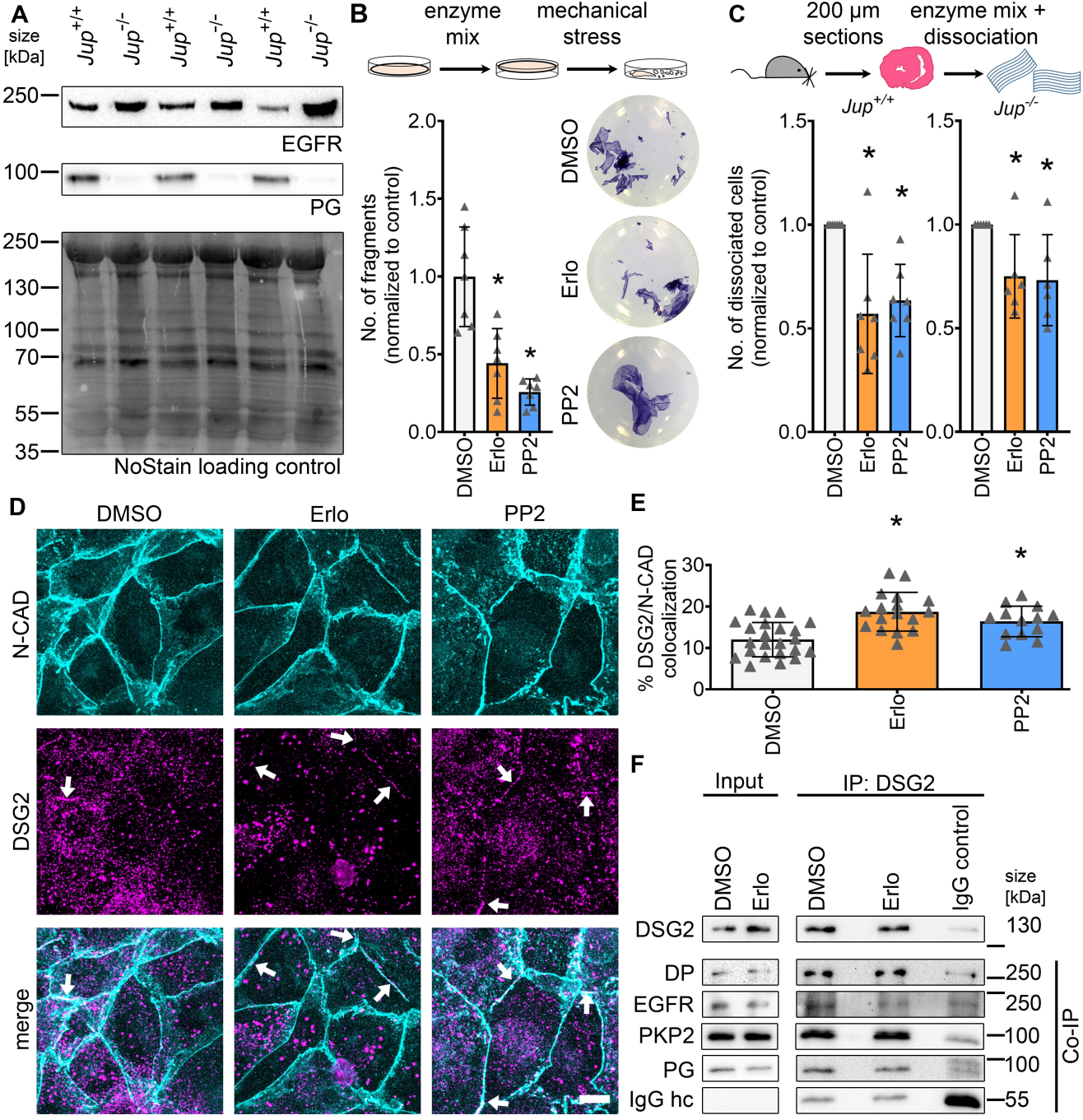
A
size [kDa]
Jup+/+
Jup-/-
Jup+/+
Jup-/-
Jup+/+
Jup-/-
250
EGFR
100
PG
250
130
100
70
55
35
NoStain loading control
B
enzyme mix
mechanical stress
No. of fragments (normalized to control)
2.0
1.5
1.0
0.5
0.0
DMSO
Erlo
PP2
C
200 µm sections
enzyme mix + dissociation
Jup+/+
Jup-/-
No. of dissociated cells (normalized to control)
1.5
1.0
0.5
0.0
DMSO
Erlo
PP2
D
DMSO
Erlo
PP2
N-CAD
DSG2
merge
E
% DSG2/N-CAD colocalization
30
20
10
0
DMSO
Erlo
PP2
F
Input
IP: DSG2
DMSO
Erlo
DMSO
Erlo
IgG control
size [kDa]
DSG2
130
DP
250
EGFR
250
PKP2
100
PG
100
IgG hc
55
Co-IP

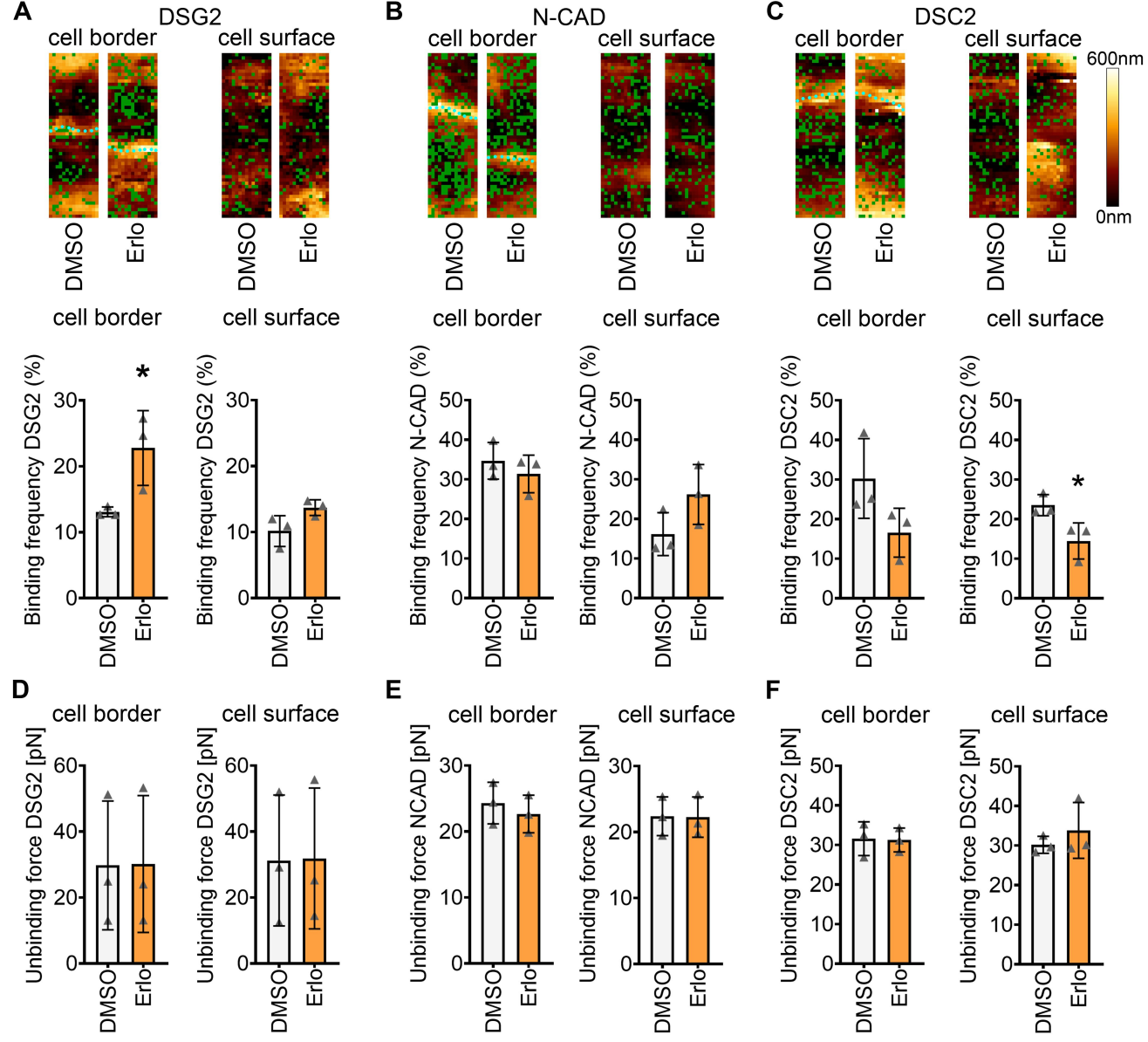
A
DSG2
cell border
cell surface
DMSO
Erlo
B
N-CAD
C
DSC2
600nm
0nm
Binding frequency DSG2 (%)
Binding frequency N-CAD (%)
Binding frequency DSC2 (%)
D
E
F
Unbinding force DSG2 [pN]
Unbinding force NCAD [pN]
Unbinding force DSC2 [pN]

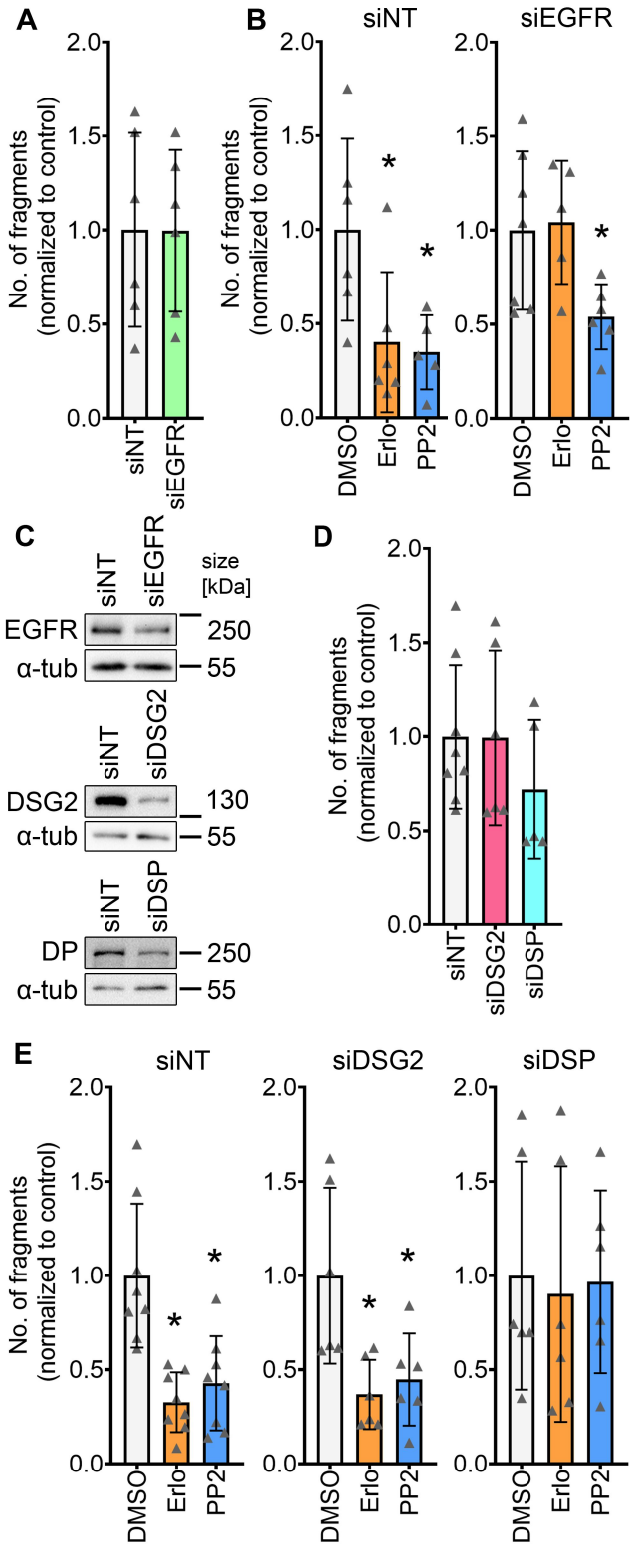
A
B
siNT
siEGFR
No. of fragments (normalized to control)
2.0
1.5
1.0
0.5
0.0
siNT
siEGFR
DMSO
Erlo
PP2
C
siNT
siEGFR
size [kDa]
EGFR
α-tub
250
55
siNT
siDSG2
DSG2
α-tub
130
55
siNT
siDSP
DP
α-tub
250
55
D
siNT
siDSG2
siDSP
E
siNT
siDSG2
siDSP

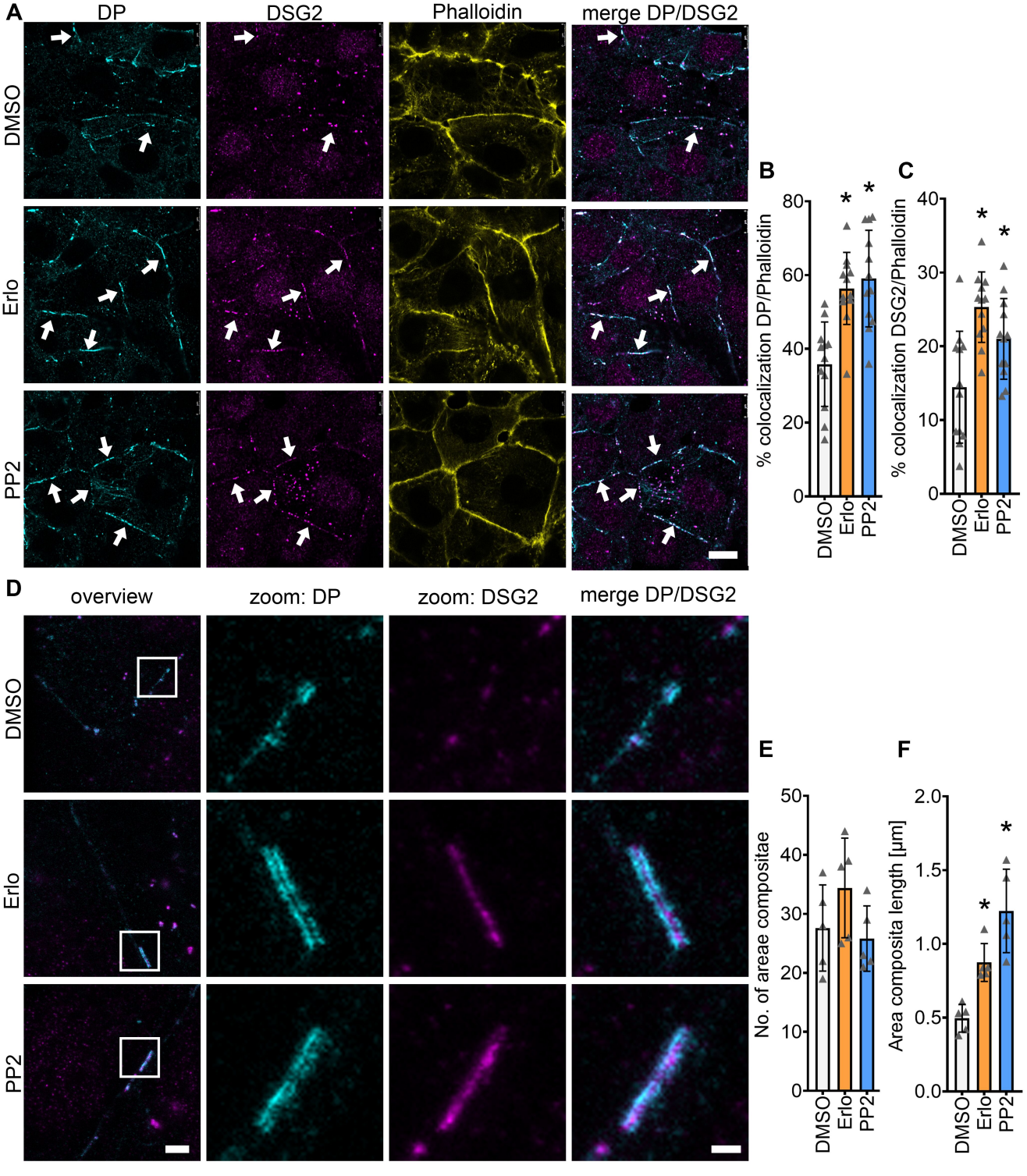
A
DP
DSG2
Phalloidin
merge DP/DSG2
DMSO
Erlo
PP2
B
% colocalization DP/Phalloidin
C
% colocalization DSG2/Phalloidin
D
overview
zoom: DP
zoom: DSG2
merge DP/DSG2
E
No. of areae compositae
F
Area composita length [µm]

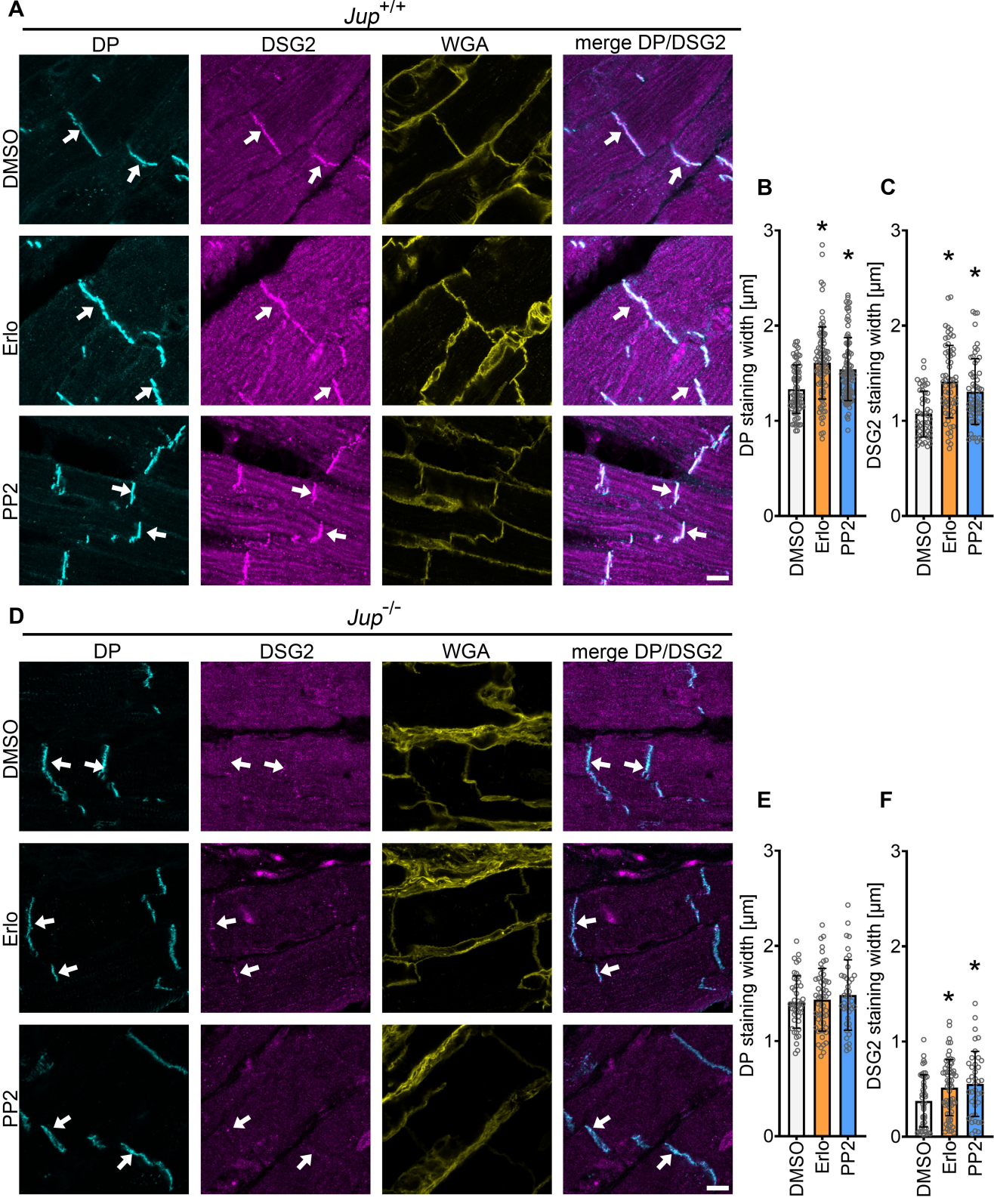
A
Jup+/+
DP
DSG2
WGA
merge DP/DSG2
DMSO
Erlo
PP2
B
DP staining width [µm]
C
DSG2 staining width [µm]
D
Jup-/-
E
F

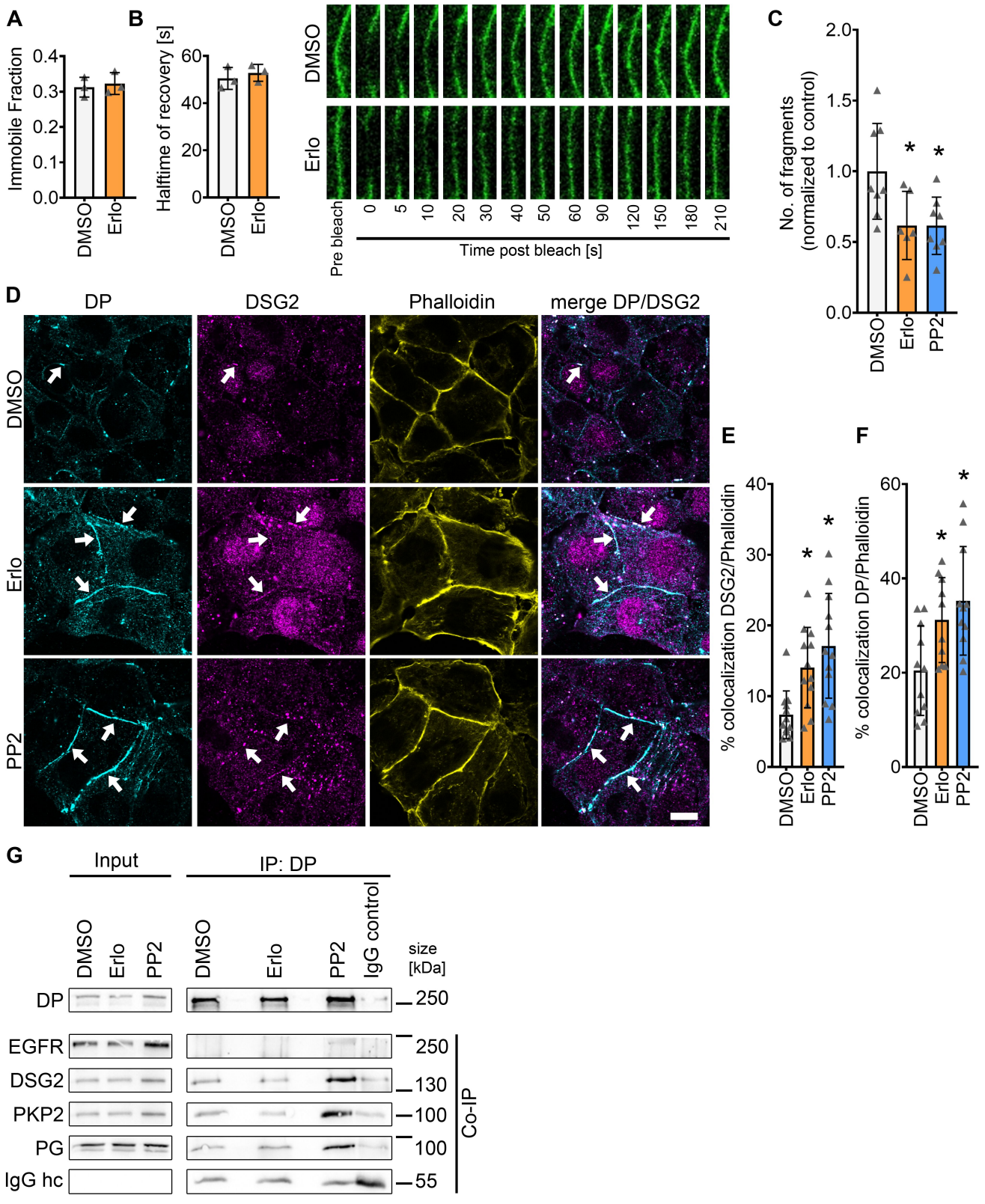
A
Immobile Fraction
0.4
0.3
0.2
0.1
0.0
DMSO
Erlo
B
Halftime of recovery [s]
60
40
20
0
DMSO
Erlo
DMSO
Erlo
Pre bleach
0
5
10
20
30
40
50
60
90
120
150
180
210
Time post bleach [s]
C
No. of fragments (normalized to control)
2.0
1.5
1.0
0.5
0.0
*
*
DMSO
Erlo
PP2
D
DP
DSG2
Phalloidin
merge DP/DSG2
DMSO
Erlo
PP2
E
% colocalization DSG2/Phalloidin
40
30
20
10
0
*
*
DMSO
Erlo
PP2
F
% colocalization DP/Phalloidin
60
40
20
0
*
*
DMSO
Erlo
PP2
G
Input
IP: DP
DMSO
Erlo
PP2
DMSO
Erlo
PP2
IgG control
size [kDa]
DP
250
EGFR
250
DSG2
130
PKP2
100
PG
100
IgG hc
55
Co-IP

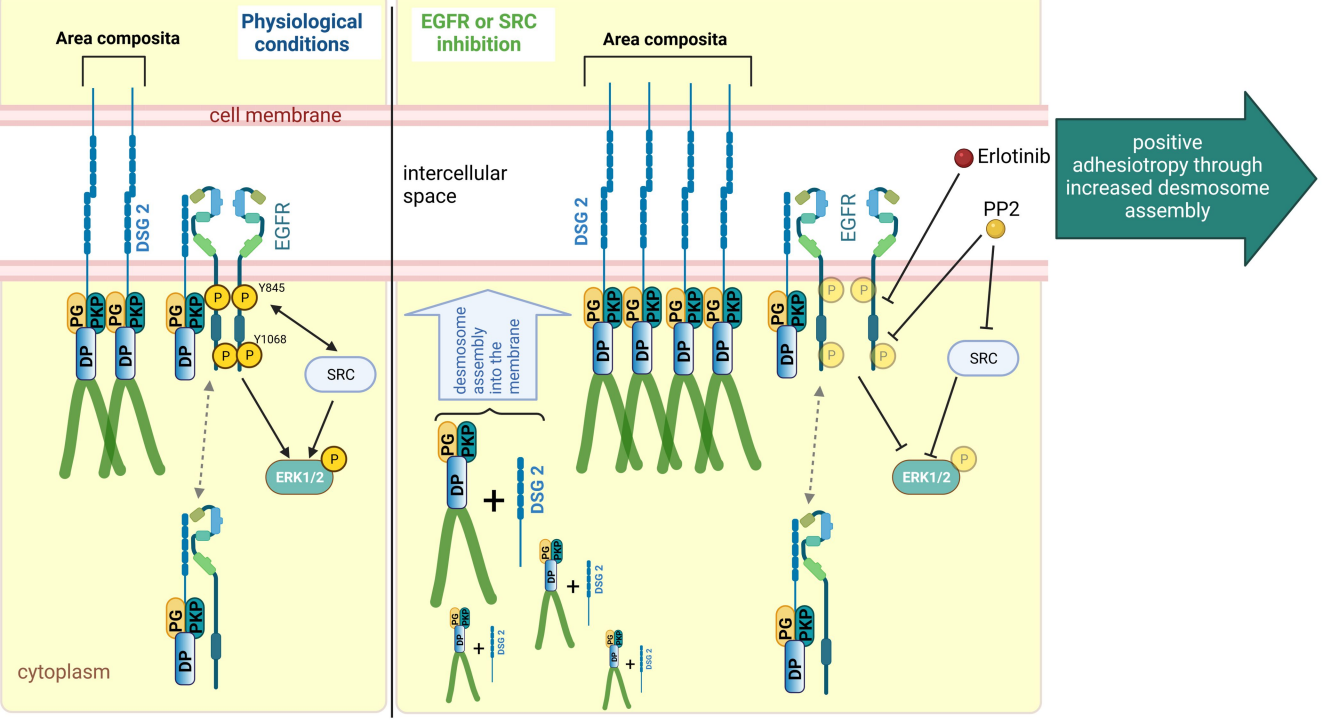
Physiological conditions
Area composita
cell membrane
DSG 2
EGFR
PG
PKP
DP
P
Y845
Y1068
SRC
ERK1/2
cytoplasm
EGFR or SRC inhibition
Area composita
intercellular space
desmosome assembly into the membrane
Erlotinib
PP2
positive adhesiotropy through increased desmosome assembly